Design of Radial Mode Piezoelectric Transformers for Lamp Ballast Applications

by

Eric Matthew Baker

Thesis submitted to the Faculty of the Virginia Polytechnic Institute and State University
in partial fulfillment of the requirements for the degree of

Master of Science
in
Electrical Engineering

Dan Y. Chen, Chairman
Fred C. Lee
Daan Van Wyk

May 7, 2002
Blacksburg, Virginia

Keywords: radial mode, piezoelectric transformer, lamp ballast

Design of Radial Mode Piezoelectric Transformers for Lamp Ballast Applications

by

Eric Matthew Baker

Dan Y. Chen, Chairman

Electrical Engineering

(ABSTRACT)

In the past, radial-mode piezoelectric transformer (Transoner®) design has been difficult due to the complex interaction between the physical and electrical circuit characteristics. Prior to a design procedure, experimental design by Face Electronics, LC led to a sample that could fit a ballast application enabling zero voltage switching (ZVS) for the semiconductors without the use of any external inductance.

In the ballast circuit, the piezoelectric transformer is used to replace the conventional inductor-capacitor resonant tank saving valuable space and expense. With ballast in mind, a design process has been developed in this thesis to optimize radial mode transformers to fit specifically tailored applications. The graphical process described, allows the engineer to design in the capability of zero voltage switching for a half-bridge drive while simultaneously providing highly efficient performance.

The problem of mounting a piezoelectric transformer to a circuit board has also been addressed in this thesis. A thermally conductive mounting technique has been developed which can enhance both the power capability and reliability of circuits utilizing these devices.

Table of Contents

Chapter 1. The Radial Mode Piezoelectric Transformer 1

1.1 Introduction 1

1.2 Theory of Operation 1

1.3 The Simplified Equivalent Circuit Model and Efficiency Considerations 3

1.4 Piezoelectric Transformer Efficiency with Consideration of Dielectric Loss 7

1.5 Summary 10

Chapter 2. Radial Mode Piezoelectric Transformer Design 11

2.1 Introduction 11

2.2 Characteristic Equations 12

2.3 Building the Output Layer 15

2.4 Adding Input Layer(s) 16

2.5 Narrowing the Range of Input Layer Thickness 19

2.6 Completing the Design 23

2.7 Experimental Results 24

2.8 Summary 27

Chapter 3. Design of a Piezoelectric Transformer Ballast 28

3.1 Introduction 28

3.2 Phase Relationship of the Drive and Output Waveforms 28

3.3 Circuit Schematic and Description 29

3.4 Circuit Test Results 33

3.5 Summary 38

Chapter 4. Thermally Conductive Mounting Technique 40

4.1 Introduction 40

4.2 Important Considerations 42

4.3 Test Results 44

4.4 Summary 45

Chapter 5. Conclusions and Future Work 46

References 48

Appendix A. Mathcad Program to Generate Two-Dimentional Projections for the VTB-1 Radial Mode Piezoelectric Transformer 50
Vita 56

List of Illustrations

Figure 1.1. Radial mode piezoelectric transformer. 1
Figure 1.2. Simplified radial mode piezoelectric transformer construction. 2
Figure 1.3. Simplified radial Mode piezoelectric transformer model. 3
Figure 1.4. One wavelength is equivalent to the cross-sectional diameter. 3
Figure 1.5. Physical construction of Transoner. 4
Figure 1.6. Piezoelectric transformer equivalent circuit model. 4
Figure 1.7. Transformed piezoelectric transformer equivalent circuit model. 5
Figure 1.8. Theoretical efficiency of the Face Electronics CZ-3 PT. 7
Figure 1.9. Theoretical efficiency of the Face Electronics CZ-3 PT including dielectric losses. 9
Figure 1.10. Efficiency difference in the CZ-3 PT when dielectric loss is both considered and disregarded. 10
Figure 2.1. Half-bridge ballast circuit topology using a Transoner. 12
Figure 2.2. Piezoelectric transformer simplified equivalent circuit model with dielectric losses and load resistance. 13
Figure 2.3. Physical dimensions of the prototype output layer. 16
Figure 2.4. Voltage gain of the prototype piezoelectric transformer versus primary layer thickness and frequency, with a single primary layer. 17
Figure 2.5. Voltage gain of the prototype piezoelectric transformer versus primary layer thickness and frequency with two primary layers. 18
Figure 2.6. Region where voltage gain is greater than the required minimum. 19
Figure 2.7. Region where inductor current is great enough to achieve ZVS. 21
Figure 2.9. Region where efficiency is greater than the preset minimum. 22
Figure 2.10. Valid choices for the prototype Transoner. 23
Figure 2.11. Physical construction of the prototype Transoner 24
Figure 2.12. Comparison of theoretical and actual ignition voltage gains. 25
Figure 2.13. Comparison of theoretical and actual steady-state voltage gains. 26
Figure 2.14. Comparison of theoretical and actual efficiency. 26

Figure 2.15. Comparison of theoretical and actual inductor current. Where each inductor current exceeds its critical line, indicates a region of possible ZVS operation given the appropriate switch dead-time. 27
Figure 3.1. Gain and phase relationship of the VTB-1 Transoner during both ignition (Av1) and full-power operation (Av2). 29
Figure 3.2. Complete non-PFC circuit schematic. 32
Figure 3.3. Input voltage and current to the non-PFC circuit. 33
Figure 3.4. Piezoelectric transformer drive voltage displaying ZVS operation. 34
Figure 3.5. Lamp driving voltage and current and lamp crest factor. 35
Figure 3.6. Operation of the non-PFC ballast. 36
Figure 3.7. Total conducted EMI measurement result during full-power operation. 37
Figure 3.8. Common mode and differential mode conducted EMI measurements result during full-power operation. 38
Figure 4.1. Radial mode piezoelectric transformer. 40
Figure 4.2. Physical construction of interface and piezoelectric transformer 41
Figure 4.3. Actual mounting of Transoner to PCB. 41
Figure 4.4. Simplified piezoelectric transformer equivalent circuit model. 42

List of Tables

Table 1.1. CZ-3 equivalent circuit model parameters. 6
Table 2.1. Material symbols and definitions. 13
Table 2.2. Design example ballast circuit specifications. 14
Table 2.3. APC-841 piezoelectric ceramic properties. 15
Table 2.4. Prototype PT theoretical equivalent circuit parameters. 24
Table 2.5. Measured VTB-1equivalent circuit parameters. 25
Table 3.1. Comparison of VTB and VTF PT measured Parameters. 31
Table 4.1. Thermal interface materials. 43

Chapter 1. The Radial Mode Piezoelectric Transformer

1.1 Introduction

The radial mode piezoelectric transformer has been well characterized in [1,6,7,8,9]. In basic terms, it is an electromechanical device, which accepts electrical energy at its input terminals and converts this to resonant mechanical energy. The mechanical energy is then reconverted back to electrical such that it can be used in an electrical circuit.

The construction of a piezoelectric transformer begins with a piezoelectric actuator as in [1,2,3]. The actuator(s) can be made up of one or more layers of piezoelectric ceramic material. The actuator(s) are then physically coupled to one or more layers called the transducer(s). Electrical energy is coupled to both the input and output layers trough the use of electrodes connected to the surface of the piezoelectric ceramic or what this thesis will refer to as piezoceramic. In the case of a radial mode piezoelectric transformer or Transoner®, the electrodes are often constructed using very thin copper. A simple diagram of such construction is shown below as Figure 1.1.

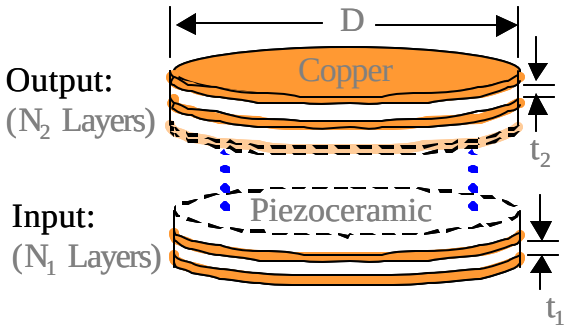

Figure 1.1. Radial mode piezoelectric transformer.

1.2 Theory of Operation

A simplified diagram of the construction of a radial mode piezoelectric actuator or transducer is shown below as Figure 1.2. As can be seen, the construction is relatively simple. Discs of piezoelectric ceramic are bonded to copper electrodes using an

adhesive. Additional piezoelectric ceramic layers can then be bonded together creating a path for the energy to be transferred between the actuator(s) and transducer(s).

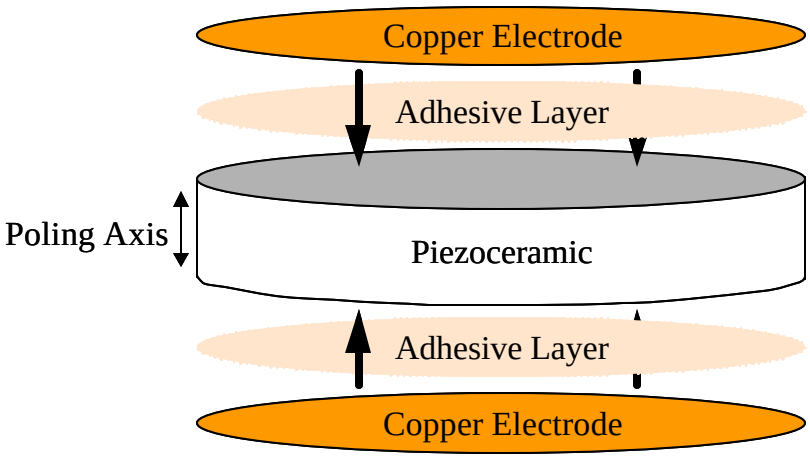

Figure 1.2. Simplified radial mode piezoelectric transformer construction.

In the case of the radial mode piezoelectric transformer, the poling axis for the piezoelectric ceramic is in the Z-direction. The piezoelectric ceramic is made to vibrate in the X and Y plane thus characterizing the type of actuator(s) and transducer(s) as transverse mode as in [1,6]. In the transverse mode, the poling axis is perpendicular to the plane or direction of vibration. By applying a voltage to the actuator or primary side of the structure, mechanical stress, T, is induced in the piezoelectric ceramic material. The mechanical stress in the actuator(s) is coupled directly to the transducer(s) through the adhesive layer(s) as shown in Figure 1.3. This stress is hence converted to an electric field across the output terminals of the device.

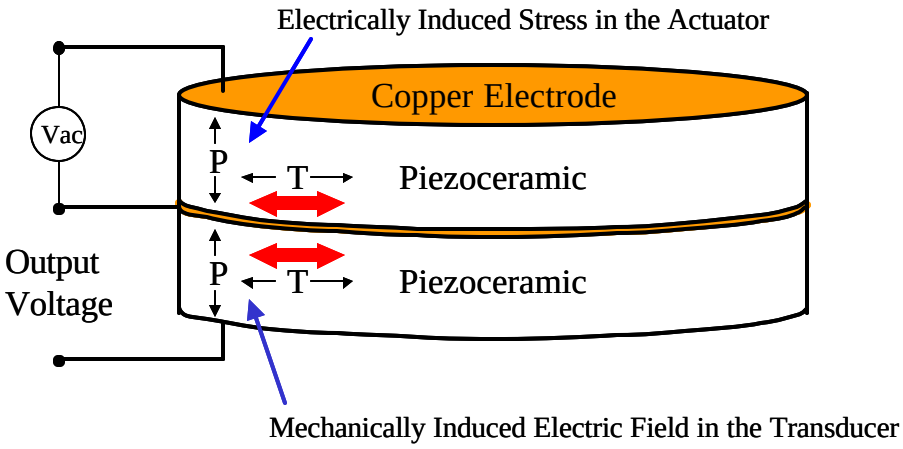

Figure 1.3. Simplified radial Mode piezoelectric transformer model.

The fundamental vibration frequency is inversely proportional to the radius and directly proportional to the wave propagation speed of the material [1,5,11,13] as shown in Equation (1.1) and Figure 1.4.

$$f_r \cong \frac{N_R}{D}$$ Where N_R is the material wave speed and D is the diameter. (1.1)

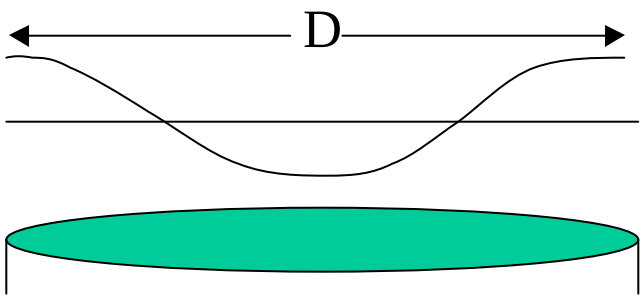

Figure 1.4. One wavelength is equivalent to the cross-sectional diameter.

1.3 The Simplified Equivalent Circuit Model and Efficiency Considerations

The accepted simplified equivalent circuit model for a piezoelectric transformer or PT has been well developed in [1,2]. This model equates to a parallel-series resonant

electrical circuit, representative of the properties exhibited by two or more layers of piezoelectric ceramic physically coupled together. Electrical connections are made through metallic physical connections on the surface of each layer. Fig. 1.5 shows a two layer Transoner and the physical electrical connections. Transoner can be constructed to have multiple primary and secondary layers of different thickness, as the application requires. Fig. 1.6 captures the simplified equivalent circuit model common to all piezoelectric transformers.

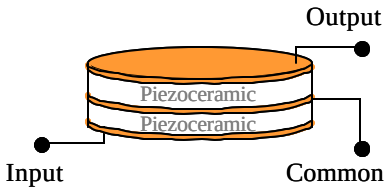

Figure 1.5. Physical construction of Transoner.

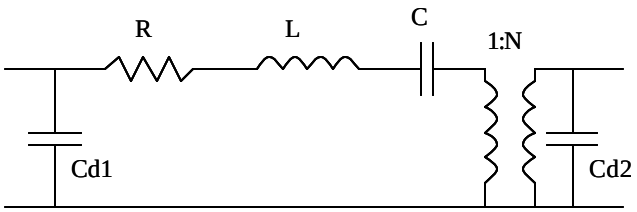

Figure 1.6. Piezoelectric transformer equivalent circuit model.

There are two defining resonant points of a piezoelectric transformer. The first is the result of when there is a short circuit applied to the output. The second occurs when there is an open circuit load. The equations defining these frequencies appear as Equations (1.2) and (1.3), respectively. Operating the piezoelectric transformer with any load resistance assures that the respective resonant frequency will appear between these two limits.

$$w_{SC} = \frac{1}{\sqrt{L \cdot C}} \tag{1.2}$$

$$w_{OC} = \frac{1}{\sqrt{L \cdot (C^{-1} + (N^2 \cdot Cd2)^{-1})^{-1}}} \tag{1.3}$$

In order to better analyze the properties of the above equivalent circuit model and a physical load, a resistor can be connected in parallel with the output capacitance, Cd2. The two components can then be transferred to the primary side of the equivalent circuit model through the turns ratio, N. For a given frequency, ω_s, the parallel connected load resistance, RL, and the output capacitance, Cd2, can be transformed to series connected equivalents, as shown in Fig. 1.7. The equations governing this impedance transformation are shown in Equations (1.4) and (1.5) for $Cd2^*$ and RL^*, respectively.

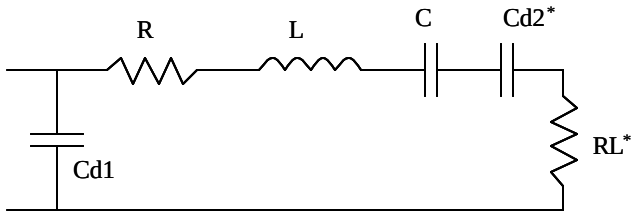

Figure 1.7. Transformed piezoelectric transformer equivalent circuit model.

$$Cd2^* = N^2 \cdot Cd2 \cdot \frac{(1 + w_s^2 \cdot RL^2 \cdot Cd2^2)}{w_s^2 \cdot RL^2 \cdot Cd2^2} \tag{1.4}$$

$$RL^* = \frac{RL}{N^2 \cdot (1 + w_s^2 \cdot RL^2 \cdot Cd2^2)} \tag{1.5}$$

Considering only real power, the ratio of the transformed load resistance, RL^*, to the sum of the series resistance, R, and RL^* yields the efficiency of the circuit. If the derivative of this ratio is considered, with respect to RL, the optimal load resistance is found to be equal to the magnitude of the capacitive reactance of the output capacitance, Cd2, as in Equation (1.6). This relationship has been well developed in [1,2,5,11,13].

$$RL = \frac{1}{w_s \cdot Cd2} \tag{1.6}$$

It should be noted that a matching network can sometimes be added between the PT and the load to increase the PT efficiency as in [1,2]. However, this technique is not considered in this thesis as it adds additional components to the design. In the design

process, covered in this thesis, it is mandated that no additional elements should be added and thus Equation (1.4) will be used as one of the constraints used in this design process for radial mode transformers.

In order to visualize the result in Equation (1.6), a three-dimensional plot can be constructed using the applied frequency, ω_s, and load resistance, RL, as the independent axes and the resulting efficiency as the dependant axis. As an example, the Face Electronics CZ-3 Transoner was chosen. The diameter of this piezoelectric transformer is 1.18-inches. There are five layers of PKI-802 piezoelectric ceramic, each measuring 0.080-inch in thickness. Four of the layers are used in parallel at the input, while a single layer is used as the output layer. The equivalent circuit model parameters are shown in Table 1.1, below.

Table 1.1. CZ-3 equivalent circuit model parameters.

Parameter	Measured Value
Cd1	10.2nF
R	901mΩ
L	1.67mH
C	2.89nF
Cd2	2.79nF
N	4.73

In Fig. 1.8 the efficiency of the CZ-3 Transoner is plotted against the load resistance, RL, and the driving frequency, f_s. By carefully following lines of constant frequency, the highest efficiency for a given frequency is achieved when the load resistance follows the formulation of Equation (1.6).

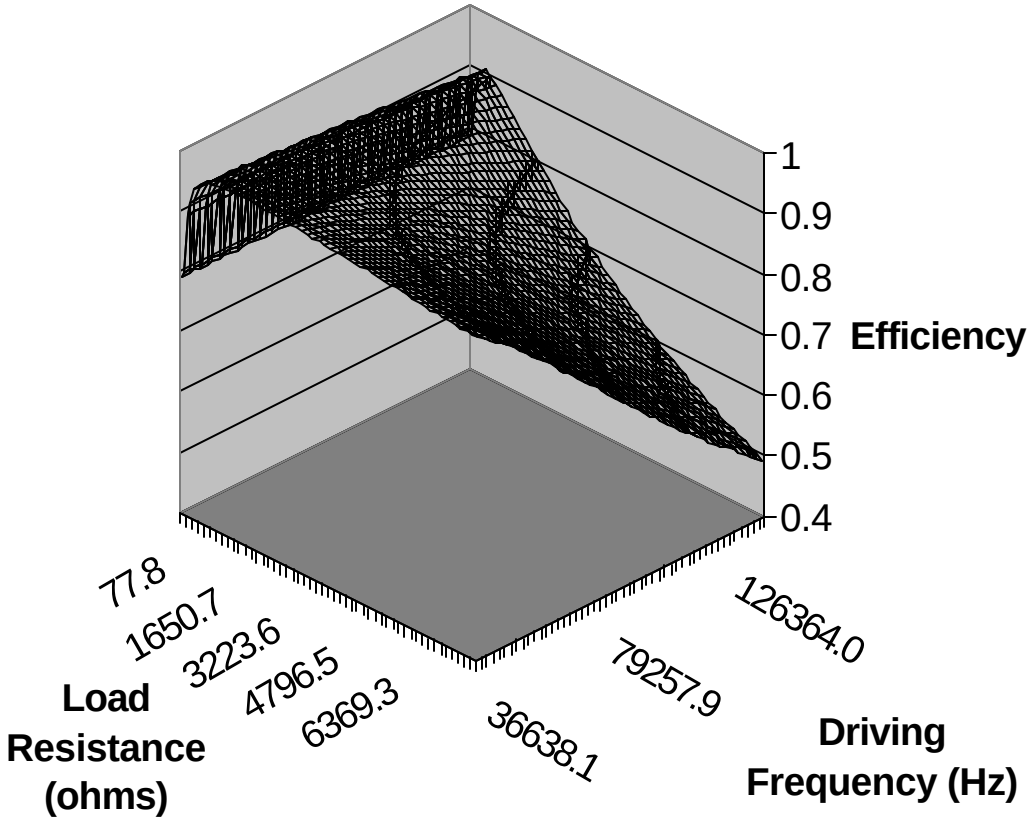

Figure 1.8. Theoretical efficiency of the Face Electronics CZ-3 PT.

1.4 Piezoelectric Transformer Efficiency with Consideration of Dielectric Loss

In order to better predict the efficiency of a piezoelectric transformer, the dielectric loss of the material should also be considered. This can be modeled as in [1,2] where the loss is seen as a frequency dependant resistance, R_{Cdx}, in parallel with both the input and output capacitances, Cd1 and Cd2. In order to calculate this loss, the dissipation factor of the piezoelectric ceramic is used as specified by the material manufacturer. Normally, the ESR or equivalent series resistance of a capacitor is shown as a series connected resistor and capacitor. This magnitude of this resistance, R_S, is a function of capacitance and the given tanδ, from the material manufacturer, as shown in Equation (1.7).

$$R_S = \frac{\tan d}{w_s \cdot Cdx} \tag{1.7}$$

In order to convert the series resistance to a parallel equivalent, one must transform the capacitance and resistance at a given frequency as in Equation (1.8). Once this transformation is complete, very small values of tanδ cause the transformation to have the form of Equation (1.9).

$$R_P = \frac{\tan d}{w_s \cdot Cdx} + \frac{1}{w_s \cdot Cdx \cdot \tan d} \tag{1.8}$$

$$R_{Cdx} = \frac{1}{w_S \cdot Cdx \cdot \tan d}. \tag{1.9}$$

The result of this added loss creates both an overall lower predicted efficiency and a change in the shape of the plot. Fig. 1.9 shows the efficiency plot including the dielectric losses of the materials. At frequencies both above and below resonant frequency range, the shape is dramatically different. Fig. 1.10 is the result of calculating the difference between the two efficiency curves (Figures 1.8 and 1.9). As can be seen, the difference is negligible near the resonant frequency range. This result is also true for any PT when the dissipation factor or tanδ of the material is relatively small, which is observed in most all piezoelectric ceramics.

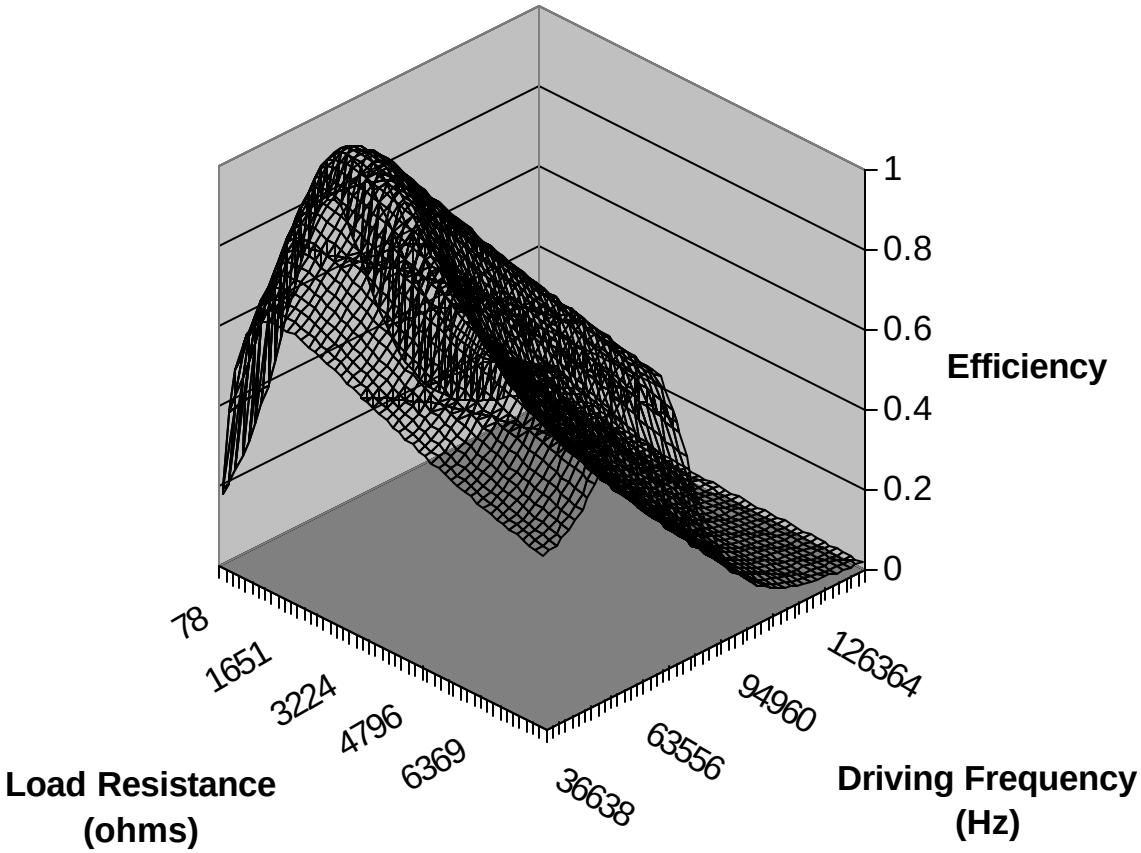

Figure 1.9. Theoretical efficiency of the Face Electronics CZ-3 PT including dielectric losses.

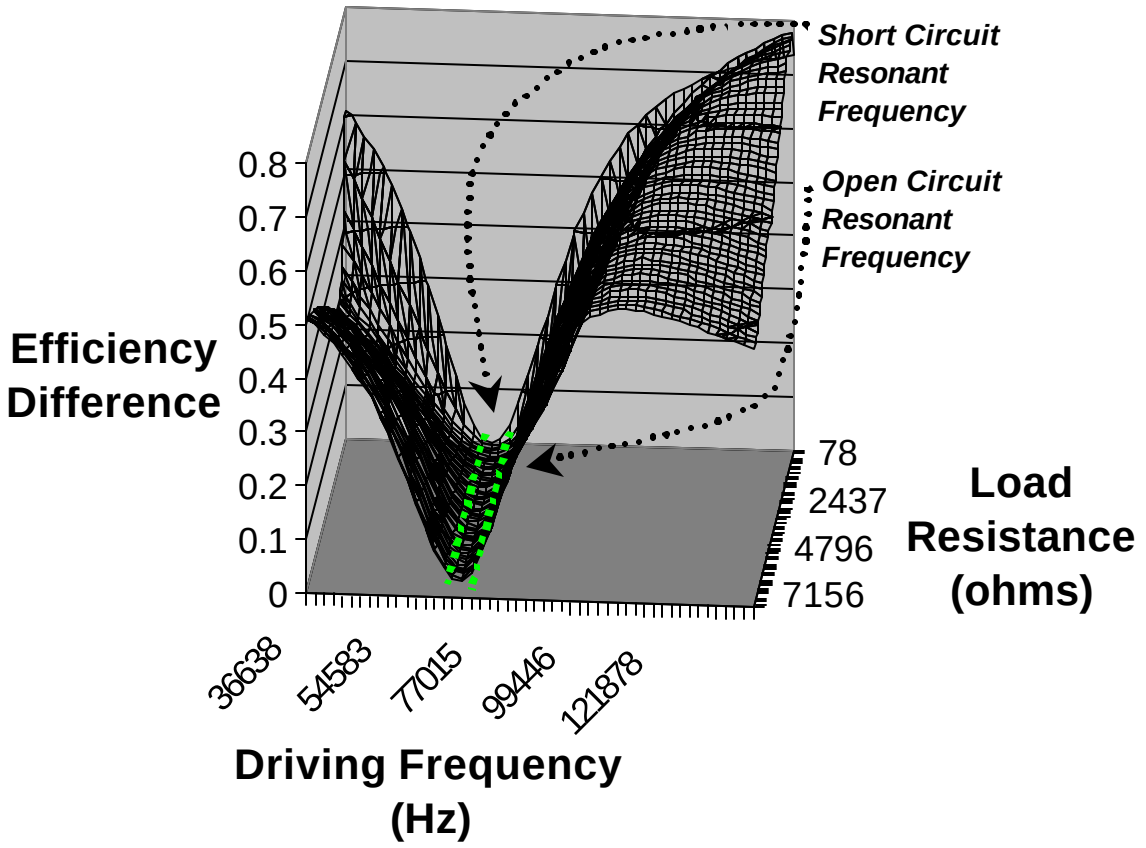

Figure 1.10. Efficiency difference in the CZ-3 PT when dielectric loss is both considered and disregarded.

If it is assumed that the piezoelectric transformer is operated at or near the resonant frequency for a particular load, the relationship described by Equation (1.7) holds true even when the dielectric losses of the material are taken into account.

1.5 Summary

This chapter has effectively introduced the radial mode piezoelectric transformer and the basic theory behind its operation and construction. The equivalent circuit of a piezoelectric transformer has also been shown to exhibit similar characteristics to a parallel-series resonant circuit, which has two distinct resonant frequencies. It has also been shown that operation at or near these frequencies results in equivalent efficiency, regardless of dielectric losses of the material.

Chapter 2. Radial Mode Piezoelectric Transformer Design

2.1 Introduction

It is commonly known that the efficacy (ratio of optical power output to electrical power input) of fluorescent lamps greatly exceeds that of the incandescent type. As a result, the heat produced by fluorescent lighting is greatly reduced for a given optical power level. It is this fact that has caused the embrace of this energy efficient form of lighting for both commercial and private use.

In order to power the simple incandescent lamp, one must only provide a voltage source, which can yield the power level prescribed by the on-state filament resistance. In contrast, fluorescent lamps require a certain voltage to ignite the lamp and a quite different voltage to sustain a given power level. This is the function of a lamp ballast circuit.

A conventional electronic ballast circuit usually consists of a parallel or series resonant converter, which contains a magnetic inductor and a high-voltage capacitor connected in series. In the ballast, a radial mode piezoelectric transformer can be utilized to replace the conventional L-C resonant tank to both save cost and weight.

Previous ballast design using the piezoelectric transformer required selecting from readily available models not always mated to a specific application. Rarely has one seen a situation in which the piezoelectric transformer could be custom designed to fit each application. In this chapter, such an endeavor has been undertaken for a 32-watt 120-volt standard line ballast. Design equations will be provided with an outline of the step-by-step procedure used in the design process. The basic circuit, shown as Figure 2.1, that is assumed in the design process has a simple half-bridge topology. An added benefit is the ability to achieve zero voltage switching for the main switches, S_1 and S_2, thus greatly aiding the efficiency of the circuit.

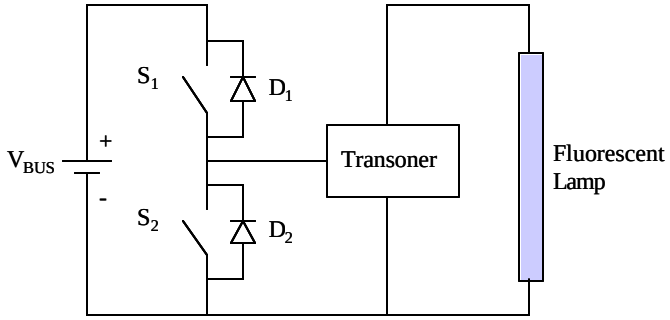

Figure 2.1. Half-bridge ballast circuit topology using a Transoner.

2.2 Characteristic Equations

The equivalent circuit model described in the previous chapter evolves from the physical construction of the piezoelectric transformer and the material characteristics [1]. Equations (2.1-2.6) show the intimate relationship between each material characteristic and physical dimension as it pertains to Transoner as developed in [1] and [11]. It has been assumed that there is perfect coupling between the layers, the copper loss is negligible, and that only the fundamental resonant mode exists. Table 2.1 contains the definitions of the various material coefficients while Figure 2.2 shows the piezoelectric transformer simplified model along with the modeled dielectric losses and load resistance, RL.

$$Cd1 = \frac{N_1 \cdot p \cdot r^2 \cdot e_{33}^T \cdot \left(1 - \frac{{d_{31}}^2}{e_{33}^T \cdot S_{11}^E}\right)}{t_1} \tag{2.1}$$

$$R = \frac{\sqrt{2 \cdot r \cdot {S_{11}^E}^3} \cdot (N_1 \cdot t_1 + N_2 \cdot t_2)}{16 \cdot r \cdot Q_m \cdot (N_1 \cdot d_{31})^2} \tag{2.2}$$

$$L = \frac{r \cdot S_{11}^{E\,2} \cdot (N_1 \cdot t_1 + N_2 \cdot t_2)}{8 \cdot p \cdot (N_1 \cdot d_{31})^2} \tag{2.3}$$

$$C = \frac{16 \cdot r^2 \cdot (d_{31} \cdot N_1)^2}{p \cdot S_{11}^E \cdot (N_1 \cdot t_1 + N_2 \cdot t_2)} \tag{2.4}$$

$$Cd2 = \frac{N_2 \cdot p \cdot r^2 \cdot e_{33}^T \cdot \left(1 - \frac{{d_{31}}^2}{e_{33}^T \cdot S_{11}^E}\right)}{t_2} \tag{2.5}$$

$$N = \frac{N_1}{N_2} \tag{2.6}$$

Table 2.1. Material symbols and definitions.

Symbol	Definition
ρ	Density
ε^T_{33}	Permittivity
Q_m	Mechanical Quality Factor
d_{31}	Piezoelectric Coefficient
S^E_{11}	Elastic Compliance
Tanδ	Dissipation Factor
N_R	Radial Mode Frequency Constant
t_1	Primary Layer Thickness
t_2	Secondary Layer Thickness
N_1	Number of Primary Layers
N_2	Number of Secondary Layers
R	Radius of the Layers

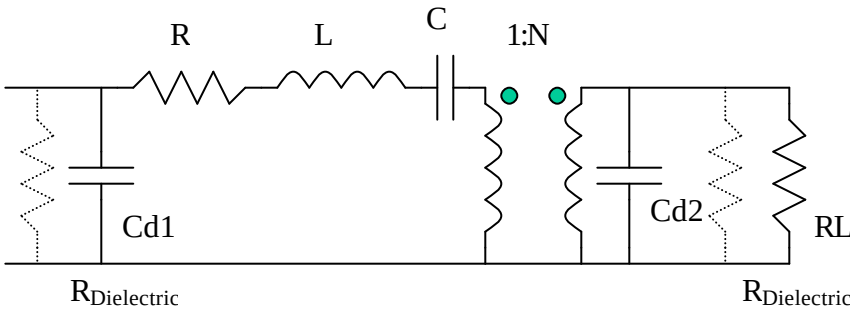

Figure 2.2. Piezoelectric transformer simplified equivalent circuit model with dielectric losses and load resistance.

The relationship described in Equation (1.6) is very important, as it initiates the Transoner design process. In order to best illustrate the design process, a specific example will be completely worked out in the body of this chapter.

Table 2.2 contains a summary of relevant circuit characteristics for a hypothetical ballast design. As is somewhat commonly known, a linear fluorescent lamp has a fixed impedance during sustained operation that can be considered resistive, as the lamp voltage and current are in phase. By utilizing Equation (1.6) and a given frequency, one can solve for the necessary capacitance, Cd2, the piezoelectric transformer should exhibit for maximum efficiency. Equation (2.7) shows this simple rearrangement.

$$Cd2 = \frac{1}{w_s \cdot RL} \tag{2.7}$$

Table 2.2. Design example ballast circuit specifications.

Specification	Value
Circuit Input Voltage	120Vrms 60Hz AC
Lamp Resistance	500 Ω
Lamp Power	32 W

Several assumptions are made during this design. The alternating voltage source will be full-bridge rectified to form the input voltage, V_{BUS}. With a reasonable amount of capacitance this source will exhibit an average of 155-volts. The circuit topology will be a simple half-bridge, as shown in Figure 2.1, which will directly drive the piezoelectric transformer. Hence, the necessary voltage gain for the device, Av_{PT}, can be calculated from the power level and the lamp resistance as in Equation (2.8). In this case, the required gain is approximately 2.0 V/V. This equation assumes a trapezoidal drive waveform at the input of the piezoelectric transformer that has a fundamental component calculated with Equation (2.9). With this in mind, the design process can begin.

$$Av_{PT} \cong \frac{\sqrt{P_{LAMP} \cdot R_{LAMP}}}{0.4 \cdot V_{BUS}} \tag{2.8}$$

$$V(n) = V_{BUS} \cdot \left(\sqrt{2} \cdot D \cdot \frac{\sin(n \cdot p \cdot D)}{n \cdot p \cdot D} \cdot \frac{\sin(n \cdot p \cdot A)}{n \cdot p \cdot A} \right) \tag{2.9}$$

Where: D = duty cycle
N = Harmonic Number
A = Ratio of the rise and fall times to the period

2.3 Building the Output Layer

As has already been shown, the approximate resonant frequency of a radial-mode piezoelectric transformer can be calculated through the use of its diameter or radius as in Equation (1.1) in the previous chapter. Table IV shows the material characteristics for APC-841 piezoelectric ceramic [16], which will be used in this design example.

Table 2.3. APC-841 piezoelectric ceramic properties.

Characteristic	Value
ρ	7.6 g/cm^3
ε^T_{33}	1350 ε_0
Q_m	1400
d_{31}	109 10^{-12} m/V
S^E_{11}	11.7 10^{-12} m^2/N
N_R	2055 m/s
tanδ	0.35 %

In this example, the diameter of the prototype piezoelectric transformer is selected to be 825-mil or 2.096-cm or 0.825-inch based on available materials and reasonable size. Ultimately the diameter should be selected through thermal analysis considering the power level and efficiency of the circuit. Solving Equation (1.1), it is found that the approximate resonant frequency, f, will be 100 kHz. Given f, Equation (2.7) can then be solved yielding the output capacitance as in Equation (2.10). Equation (2.5) can then be utilized to yield the thickness of the secondary layer(s). For this example N_2 is chosen to

be unity for simplicity. The result can be seen in Equation (2.11). Figure 2.3 shows the completed output layer planned construction.

$$Cd2 = \frac{1}{w_r \cdot R_{LAMP}} = 3.2nF \tag{2.10}$$

$$t_2 = \frac{N_2 \cdot p \cdot r^2 \cdot e_{33}^T \cdot \left(1 - \frac{d_{31}^{\ 2}}{e_{33}^T \cdot S_{11}^E}\right)}{Cd2} \cong 0.050in \tag{2.11}$$

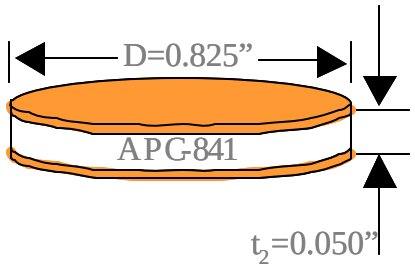

Figure 2.3. Physical dimensions of the prototype output layer.

2.4 Adding Input Layer(s)

By adding an input layer, the equivalent circuit model can be calculated. The voltage gain of the Transoner can then be plotted as a function of both driving frequency, f_s, and primary layer thickness, t_1, by calculating the complete equivalent circuit model as a function of t_1, utilizing Equations (2.1-2.6). A practical range of material thickness is from 10-mil to 200-mil. Figure 2.4 shows the resulting plot in three-dimensions. The minimum voltage gain required for this design was calculated to be 2.0 V/V from Equation (2.8). As can be seen, there is no primary layer thickness within the range that can be selected to provide this magnitude of gain.

In order to increase the voltage gain, one method is to increase the internal turns ratio within the equivalent circuit model by adding primary layers. This process can be

repeated until the voltage gain is as desired. In this case, only two primary layers were needed. The resulting voltage gain plot can be seen in Figure 2.5.

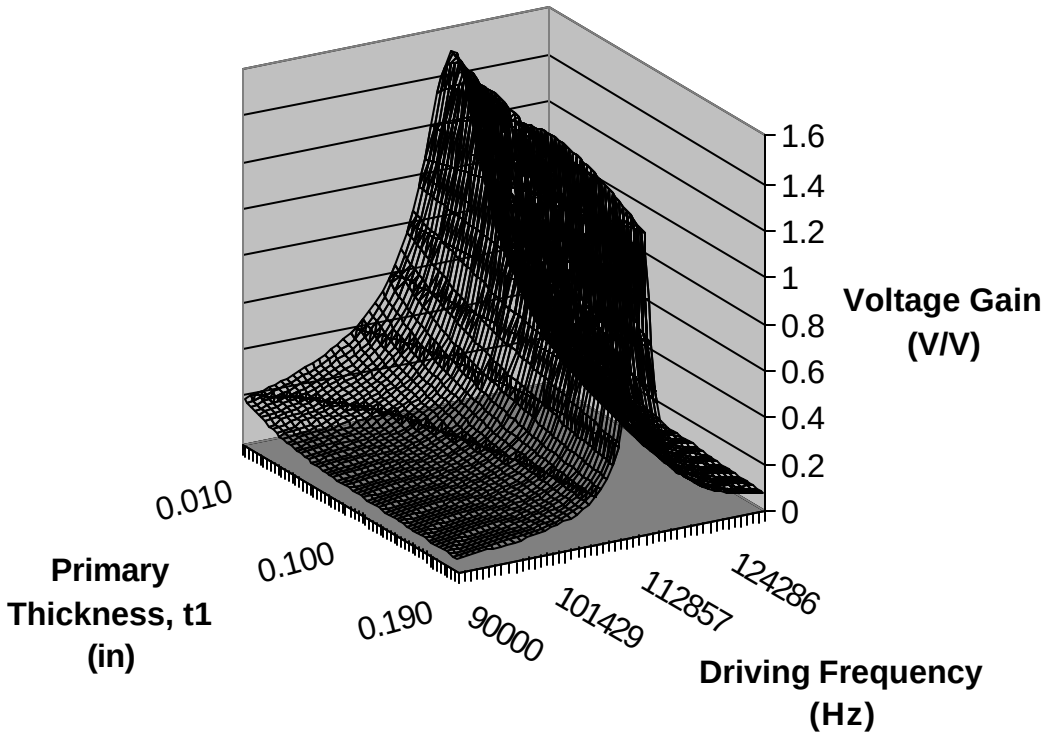

Figure 2.4. Voltage gain of the prototype piezoelectric transformer versus primary layer thickness and frequency, with a single primary layer.

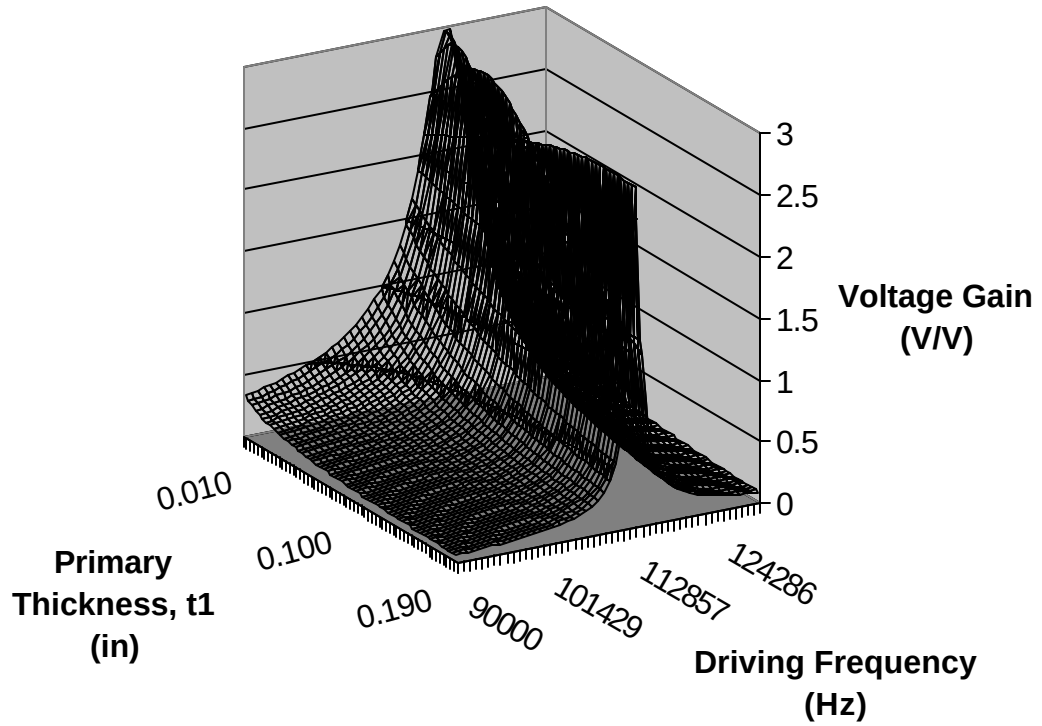

Figure 2.5. Voltage gain of the prototype piezoelectric transformer versus primary layer thickness and frequency with two primary layers.

By taking a slice of the plot at the minimum required voltage gain, a two-dimensional surface projection can be generated which allows one to easily see where, in the (t_1 x f_s) plane, a solution exists. Using this technique Figure 2.6 was generated.

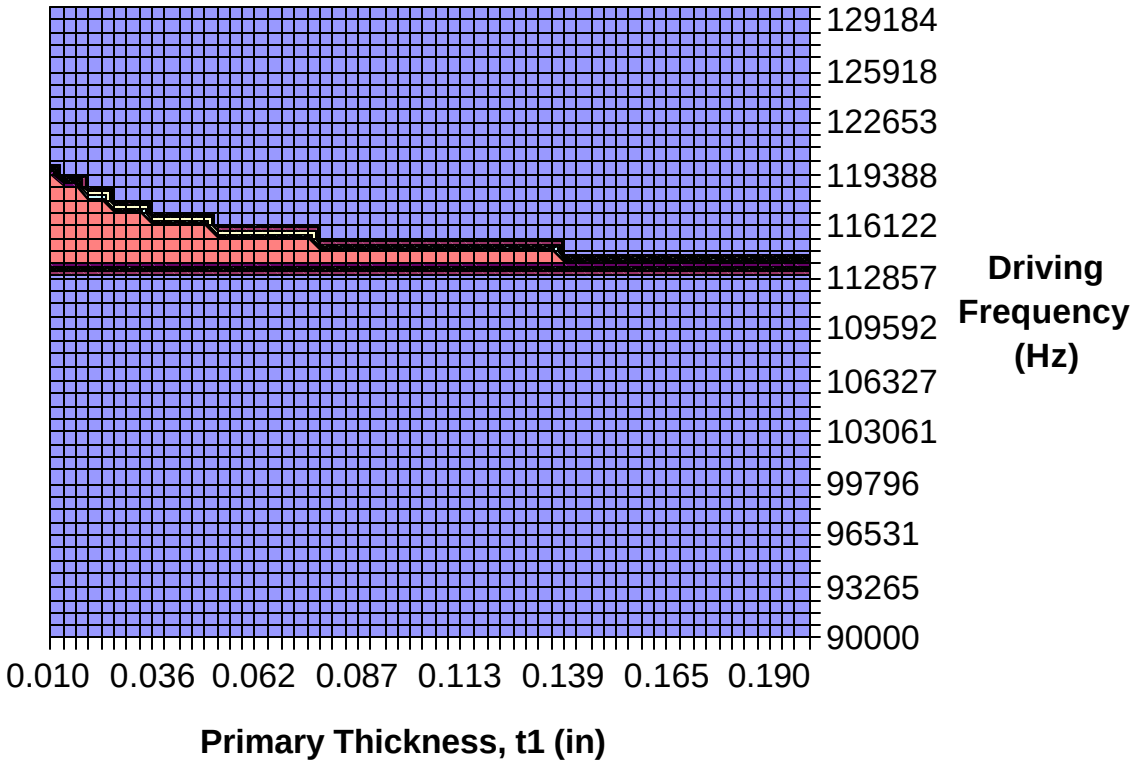

Figure 2.6. Region where the voltage gain is greater than the required minimum.

2.5 Narrowing the Range of Input Layer Thickness

In analyzing Figure 2.6, it can be seen that the entire range of primary layer thickness can meet the voltage gain requirement. In order to narrow down a smaller range of thickness, more constraints must be included.

With the choice of a half-bridge topology, zero voltage switching can be achieved for the two switches, S_1 and S_2, if enough dead time is provided and the relationship seen as (17) is met [1]. In short, the energy within the internal inductance, L, should be great enough to charge/discharge the internal capacitance, C, and the input capacitance, Cd1, during the dead-time period. Using the energy stored in both the capacitors and inductor and charge equivalence as seen in Equations (2.12-2.13) and, one can develop Equation (2.14). By solving for the internal inductor current, a critical value, shown as Equation (2.15), evolves which must be surpassed in order for ZVS to take place. The peak inductor current can be approximated through the use of Equation (2.16) as in [5,10]

where Z_{in} is the input impedance of the piezoelectric transformer excluding Cd1, but including the lamp load, and d is the duty cycle of each switch. Using the same technique as Figure 2.6, a three-dimensional plot of the peak inductor current has been sliced where it exceeds the minimum or critical value and is shown as Figure 2.7 plotted against both input layer thickness and driving frequency.

$$\frac{1}{2}\cdot L\cdot \Delta i_{Lpeak}^{2} \geq \frac{1}{2}\cdot Cd1\cdot Vbus^{2} + \frac{1}{2}\cdot C\cdot V_{C}^{2} \tag{2.12}$$

$$Q = Cd1\cdot Vbus = C\cdot V_{C} \Rightarrow V_{C} = \frac{Cd1\cdot Vbus}{C} \tag{2.13}$$

$$\frac{1}{2}\cdot L\cdot \Delta i_{L\,peak}^{\;2} \geq \frac{1}{2}\cdot Cd1\cdot Vbus^{2}\cdot\left(1+\frac{Cd1}{C}\right) \tag{2.14}$$

$$\Delta i_{L\,peak} \geq \sqrt{\frac{Cd1\cdot(C+Cd1)}{L\cdot C}}\cdot Vbus \tag{2.15}$$

$$\Delta i_{L\,peak}(f_s) = \frac{2\cdot Vbus}{p\cdot\left|Z_{in}(f_s)\right|}\cdot\frac{\sin(p\cdot d)}{p\cdot d}\sin(\angle Z_{in}(f_s)) \tag{2.16}$$

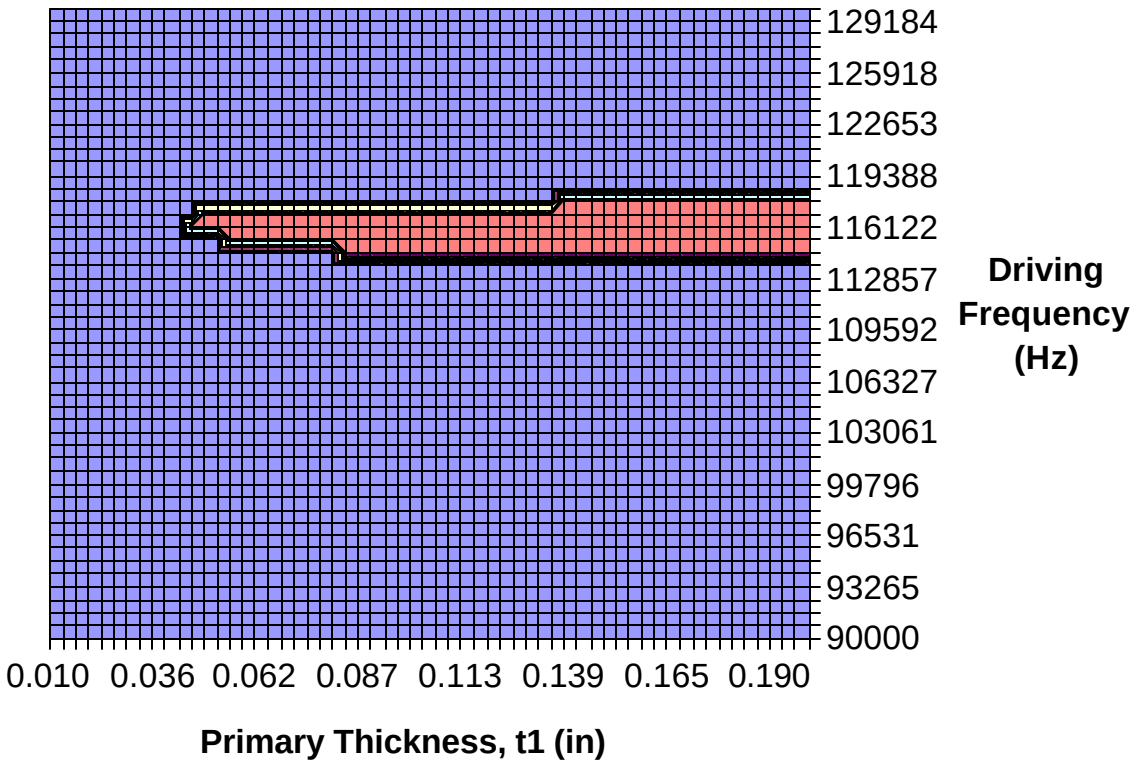

Figure 2.7. Region where inductor current is great enough to achieve ZVS.

In order to further narrow the choices of input layer thickness, one can put a minimum on the efficiency tolerable in the circuit. To better enhance the appeal of using a piezoelectric transformer in place of the conventional L-C resonant tank, the efficiency of the circuit should not be sacrificed. Calculation of the efficiency is easily accomplished by taking the quotient of the real output power over the real input power. The efficiency of the prototype then can be plotted in three-dimensions with both the primary layer thickness and frequency as the dependent axes. A limit can be set for the minimum allowable efficiency based on the Transoner size and power level. Here, a limit was set at 90% or better and the efficiency plot was then sliced at this level allowing a two-dimensional projection as before. This plot is shown as Figure 2.8.

In order to create the smallest range of choices for primary layer thickness, the three plots are then overlapped to find the common choices of both input layer thickness

and driving frequency, which are elements of all three two-dimensional projections. Any choice within this overlapped region will provide a useful piezoelectric transformer for the application. Primary thickness, t_1, should be made as small as possible within the region of solution such that the finished Transoner has minimal interference between vibration modes [1]. Figure 2.9 shows the complete common solution region.

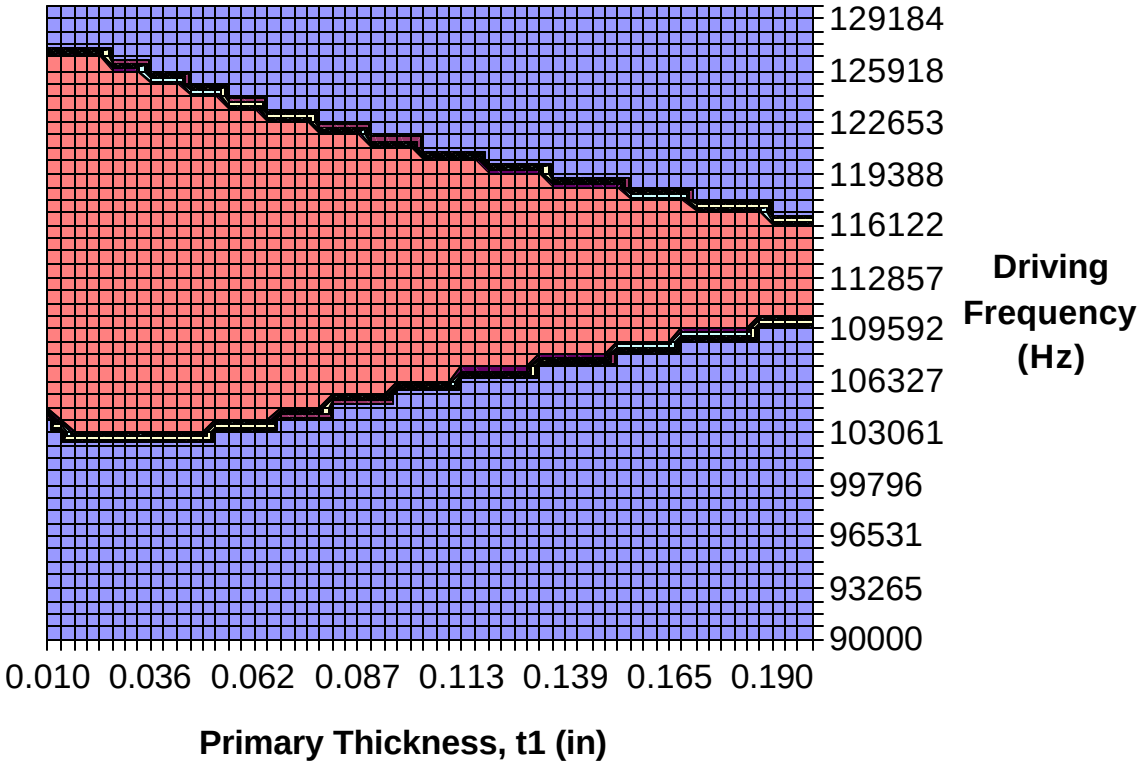

Figure 2.9. Region where efficiency is greater than the preset minimum.

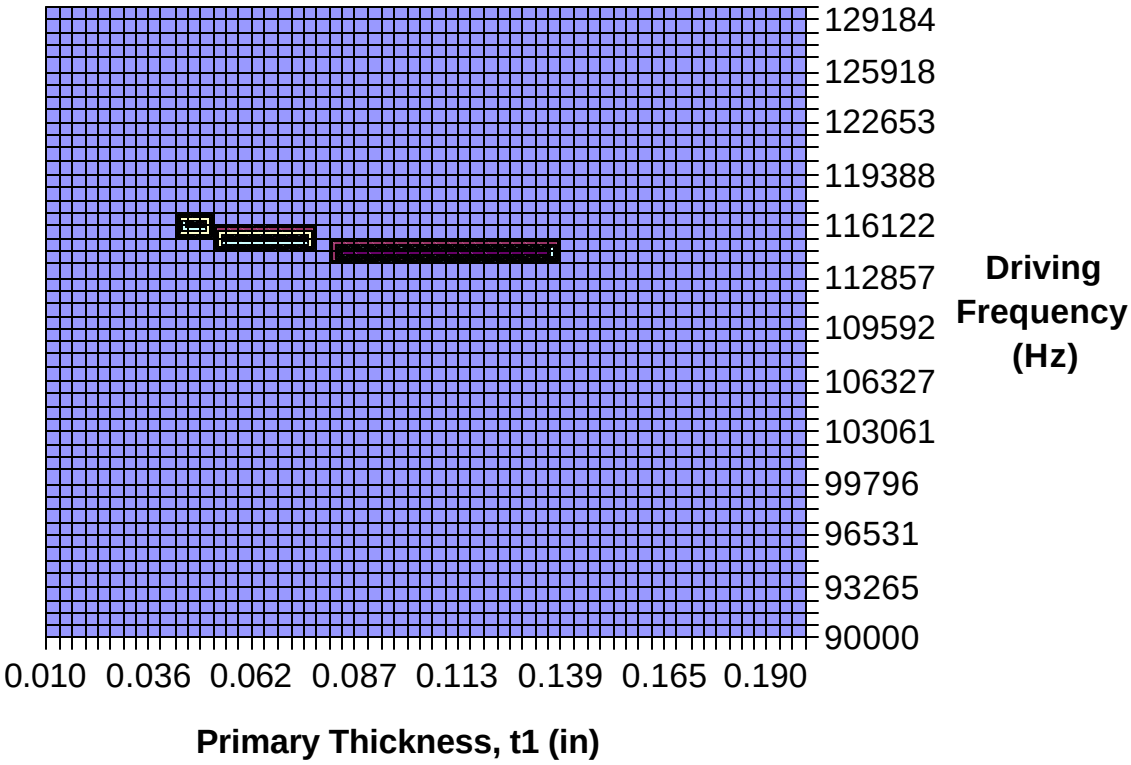

Figure 2.10. Valid choices for the prototype Transoner.

2.6 Completing the Design

From Figure 2.10, the range of primary layer thickness, which will work with our circuit, varies over quite a large range. This range may be further narrowed by increasing the level of the efficiency minimum or by placing other constraints on the design. For this example, the primary thickness was chosen to be 60-mil. Thus, the complete Transoner has two primary layers of 60-mil each and a secondary layer of 50-mil. The overall diameter is 825-mil. A simple diagram of the prototype is shown as Figure 2.11 with the theoretical equivalent circuit model parameters shown within Table 2.4.

In addition to these three main constraints in the design process, one must also consider the striking voltage necessary to ignite a fluorescent lamp. The striking voltage can be in the range of four to five times the sustaining voltage. However, as long as the efficiency of the device is designed to be fairly high, the voltage gain of the designed device will be more than adequate to ignite the lamp. In this case, a very high quality

factor parallel resonant tank is created with the internal resistance acting as the damping element.

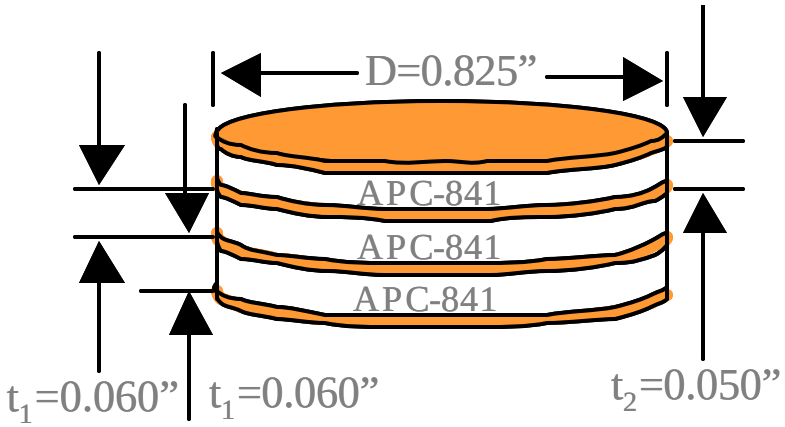

Figure 2.11. Physical construction of the prototype Transoner.

Table 2.4. Prototype PT theoretical equivalent circuit parameters.

Parameter	Value
Cd1	4.96 nF
R	1.91 Ω
L	3.78 mH
Ca	527 pF
Cd2	2.97 nF
N	2

2.7 Experimental Results

In order to verify the design procedure, Face Electronics manufactured the sample described in this design procedure designating it as Transoner VTB-1. The measured equivalent circuit parameters appear in Table 2.5. As can be seen, most all of the parameters match very well except for the equivalent internal inductance and capacitance. One possible reason for this difference is that the Transoner design equations assume perfect coupling between the primary and secondary layers. In addition, the manufacture requires the addition of copper layers and adhesive, which may alter the performance of the complete piezoelectric transformer.

Table 2.5. Measured VTB-1equivalent circuit parameters.

Parameter	Value
Cd1	4.61 nF
R	2.21 Ω
L	2.36 mH
Ca	930 pF
Cd2	2.90 nF
N	2.08

Further analysis reveals that the predicted performance of the theoretical model and the measured model is very close. Fig. 2.12 shows the performance of both the theoretical and actual measured equivalent models during the lamp ignition period. During this state, the lamp provides a very high impedance causing the resonant circuit to operate in a high quality factor parallel resonant state. The extremely high voltage gain of both models can provide more than enough striking voltage to the lamp.

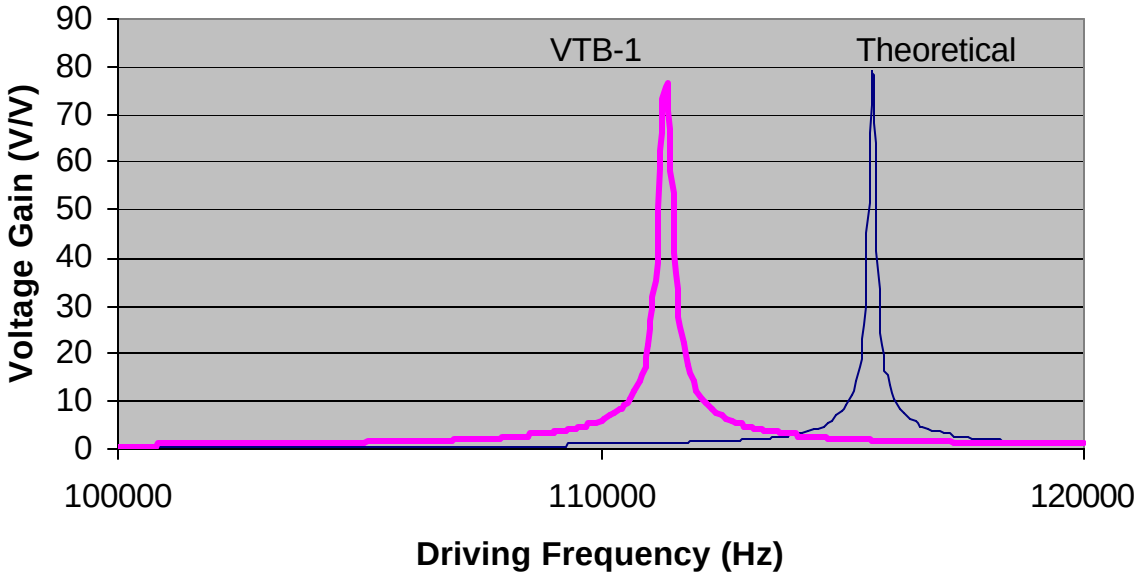

Figure 2.12. Comparison of theoretical and actual ignition voltage gains.

Figures. 2.13-2.15 show both the theoretical and actual performance, based on the equivalent circuit models, predicting voltage gain during steady state operation, efficiency, and inductor current, respectively, when a resistive load of 500-ohms is attached to the outputs. As can be seen from these plots, the only major difference in performance is where frequency is concerned. The VTB-1 Transoner has a resonant frequency of approximately 5 kHz less than the theoretical prediction.

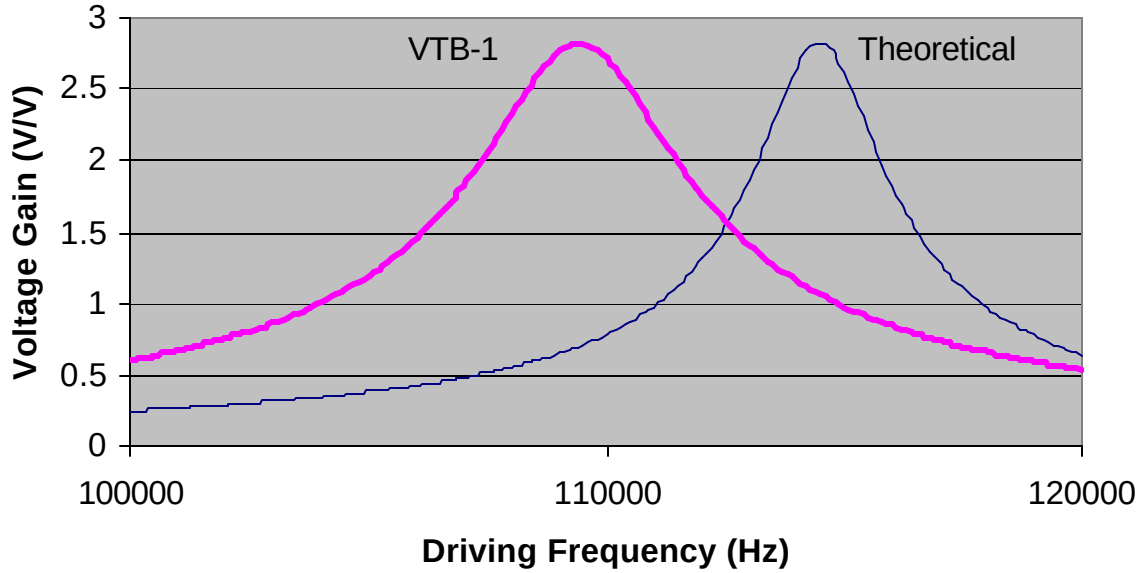

Figure 2.13. Comparison of theoretical and actual steady-state voltage gains.

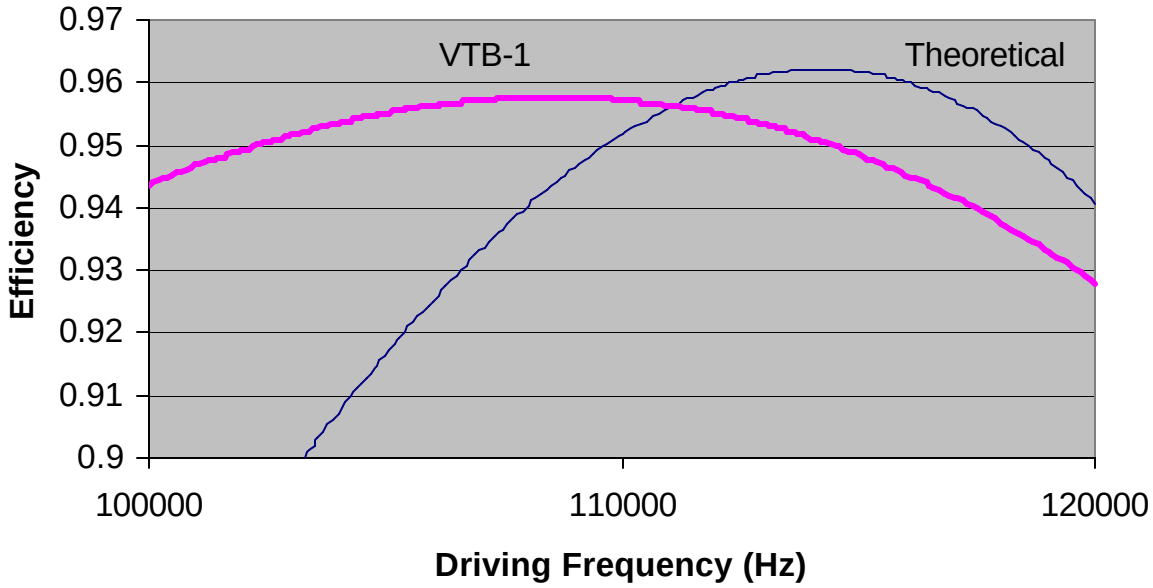

Figure 2.14. Comparison of theoretical and actual efficiency.

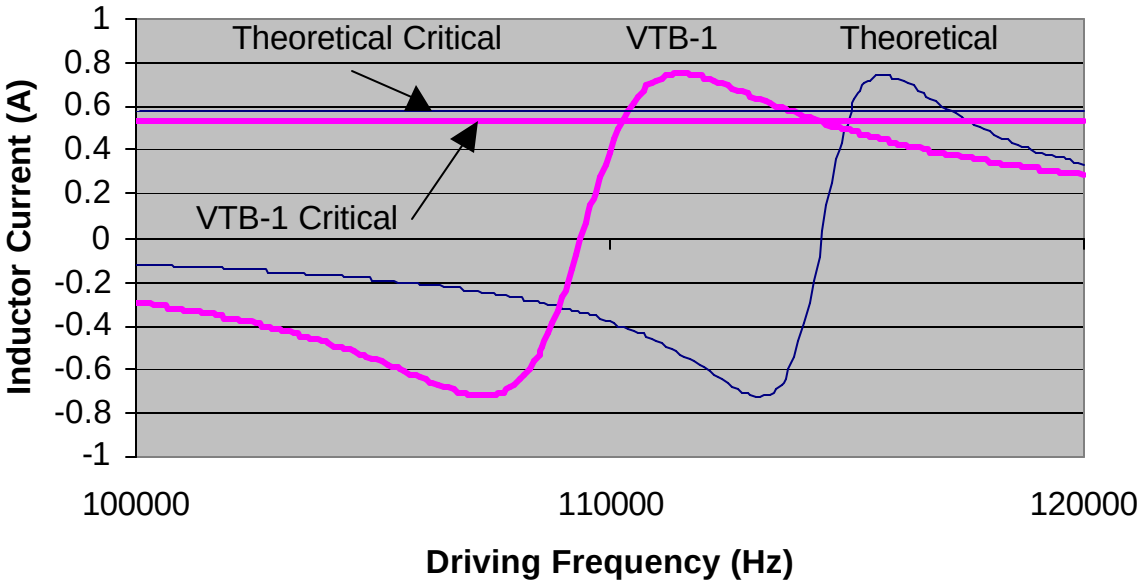

Figure 2.15. Comparison of theoretical and actual inductor current. Where each inductor current exceeds its critical line, indicates a region of possible ZVS operation given the appropriate switch dead time.

2.8 Summary

In the body of this chapter, the physical characteristics of the radial mode piezoelectric transformer have been explored. The design equations have been revealed allowing the calculation of an equivalent circuit model based on the material properties and physical dimensions. A sample was designed to meet voltage gain, ZVS operation, and high efficiency for a 120-volt 60Hz AC input application. This sample was constructed by Face Electronics and tested comparing very well the theoretical calculations.

Chapter 3. Design of a Piezoelectric Transformer Ballast

3.1 Introduction

In Chapter 2, the VTB-1 radial mode piezoelectric transformer or Transoner was designed to operate with high efficiency while driving an FHF-32 lamp and simultaneously providing a zero voltage switching condition for the half-bridge switches. In order to fully utilize the characteristics of the Transoner, a circuit control technique was developed which could not only reliable ignite a fluorescent lamp, but is could also regulate the output current and thus provide constant power under a range of input voltage conditions.

3.2 Phase Relationship of the Drive and Output Waveforms

Shown below as Figure 3.1, are the gain and phase relations ships of the VTB-1 Transoner designed as the example within Chapter 1. The plots labeled with the designation Av_1 were generated with 1-Megaohm of resistance at the output terminals. This condition simulates the load seen by the Transoner during an ignition period. Here the gas within the lamp has not been ionized and hence represents and almost infinite load impedance. The plots designated with Av_2 simulate the load conditions of the FHF-32 lamp under full-power load conditions or approximately 450-ohms.

Careful analysis of the plots shows a 90^o phase relationship exits between the input and output voltage during the ignition period at the gain peak. Unfortunately, due to the characteristics of a parallel-series resonant converter, the steady state phase relationship at the gain peak is closer to 40^o. However, one can also notice that if the phase relationship were locked to 40^o during the ignition period, the voltage gain would be very close to the peak.

Utilizing this basic idea, a circuit utilizing a CMOS-based 4046 90^o phase-locked loop [14] was created. By limiting the frequency range from 100-120kHz, the driving frequency of the piezoelectric transformer would completely encompass the VTB-1's

operational range. By locking the phase to approximately 40° instead of 90° the control loop can be made very simple. Maximum current capability would naturally occur at the voltage gain peak, thus in order to reduce or regulate the current, the frequency only needs to be raised until the current decreases to the desired level.

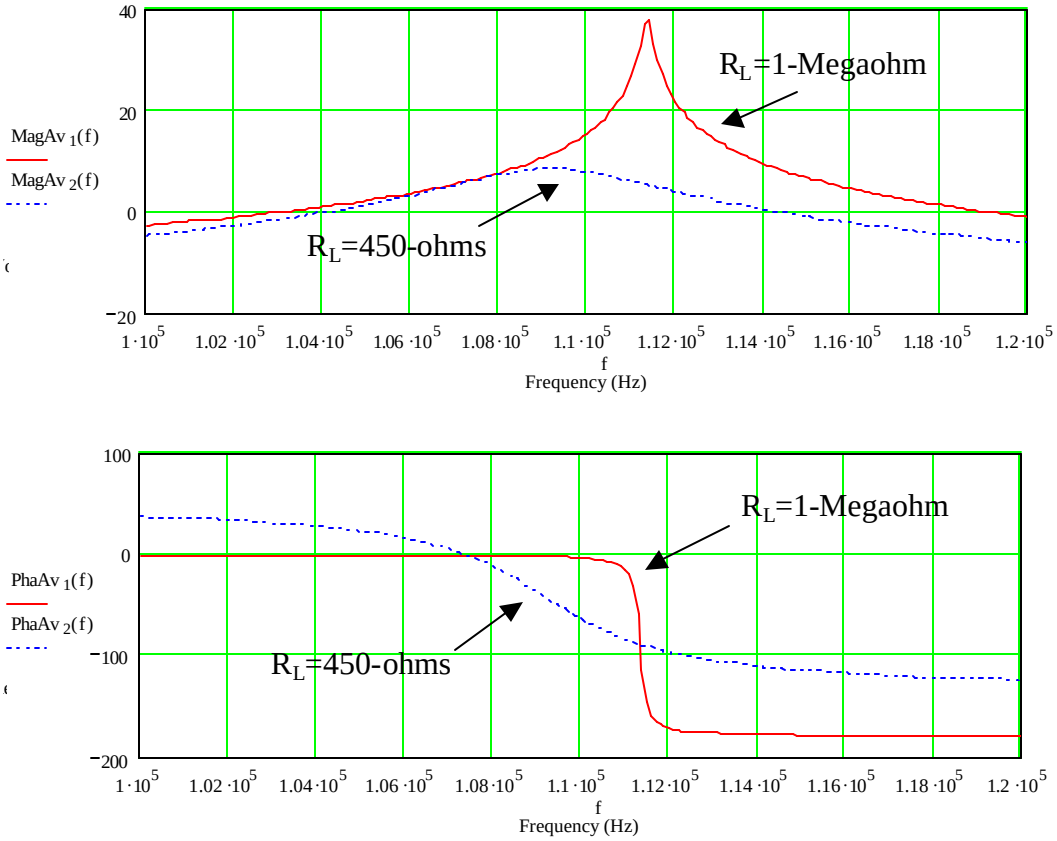

Figure 3.1. Gain and phase relationship of the VTB-1 Transoner during both ignition (Av1) and full-power operation (Av2).

3.3 Circuit Schematic and Description

Figure 3.2 below shows the complete schematic for the prototype ballast. There are basically four definable sections to this circuit. The first section functions to directly rectify the 120-volt 60-Hz AC line voltage and create the bus voltage which has an average of around 155-volts in the circuit. The next definable stage to the circuit includes a secondary full-bridge rectifier, which has series connected capacitors, which serve to limit the charge passed to the logic voltage regulator. Using this method the efficiency of

the logic power supply can be greater than a simple linear regulator connected from the bus voltage.

The third obvious section of the circuit provides control. As described above, a 90^o phase locked loop is used to ensure quick and reliable ignition of the lamp. The phase locking point is actually modified by the 39k-ohm resistor connected between the VCO_{in} pin and ground. The presence of this resistor creates a 40^o relationship between the input and output ensuring, that during the operational condition of the lamp, the peak of the voltage gain is available under full load conditions. The maximum and minimum frequencies can be set on the CD4046 chip using two external resistors and on capacitor. The equations that govern this operation are shown below as (20) and (21). Using these equations the operational frequency limits were set to 100-120kHz, with the 32-watt operation point being 111-112kHz.

$$f_{\min} = \frac{1}{R_2 \cdot (C + 32\,pF)} \qquad \text{when } VCO_{in} = Vss \tag{20}$$

$$f_{\max} = \frac{1}{R_1 \cdot (C + 32\,pF)} + f_{\min} \qquad \text{when } VCO_{in} = Vcc \tag{21}$$

The half-bridge voltage and the lamp voltage are both sampled for their respective phase information. Filtering is accomplished with a simple capacitive coupled clipping network and a series of NAND gates, which sharpen the phase signal edges and reduce noise.

The second portion of the control for this circuit regulates the lamp current by sampling and rectifying the voltage across a shunt resistor. By comparing this averaged peak current to a reference, the reference voltage for the voltage controlled oscillator built in to the CD4046 chip [14] can be increased thus increasing the oscillator frequency and hence moving the operation point to the left of the piezoelectric transformer resonance frequency. This method reduces the current into the lamp until the error voltage is zero or until the reference voltage is equal to the average peak voltage sampled across the shunt resistor.

The last section involves the L6384 half-bridge driver [15], the MOSFETs, and piezoelectric transformer. In this schematic, the Transoner selected for this circuit was actually a VTF model provided by Face Electronics, LC. As stated in the design portion of this report, the VTB model has a diameter of 825-mil, two input layers of 60-mil thickness, and a single output layer of 50-mil. The VTF model differs only in its output section. This particular model has an output section of 60-mil, which decreases the output capacitance and also slightly increases the internal resistance, R. Table 3.1 below shows the measured y-parameter equivalent circuit parameters for both the VTB and the VTF Transoner. Analysis of the differences between the performance characteristics of the VTB and VTF model is negligible, thus the in-circuit performance is almost identical.

Table 3.1. Comparison of VTB and VTF PT measured Parameters.

Parameter	VTB	VTF
Cd1	4.61 nF	4.55 nF
R	2.21 Ω	2.28 Ω
L	2.36 mH	2.54 mH
Ca	930 pF	868 pF
Cd2	2.90 nF	2.34 nF
N	2.08	2.07

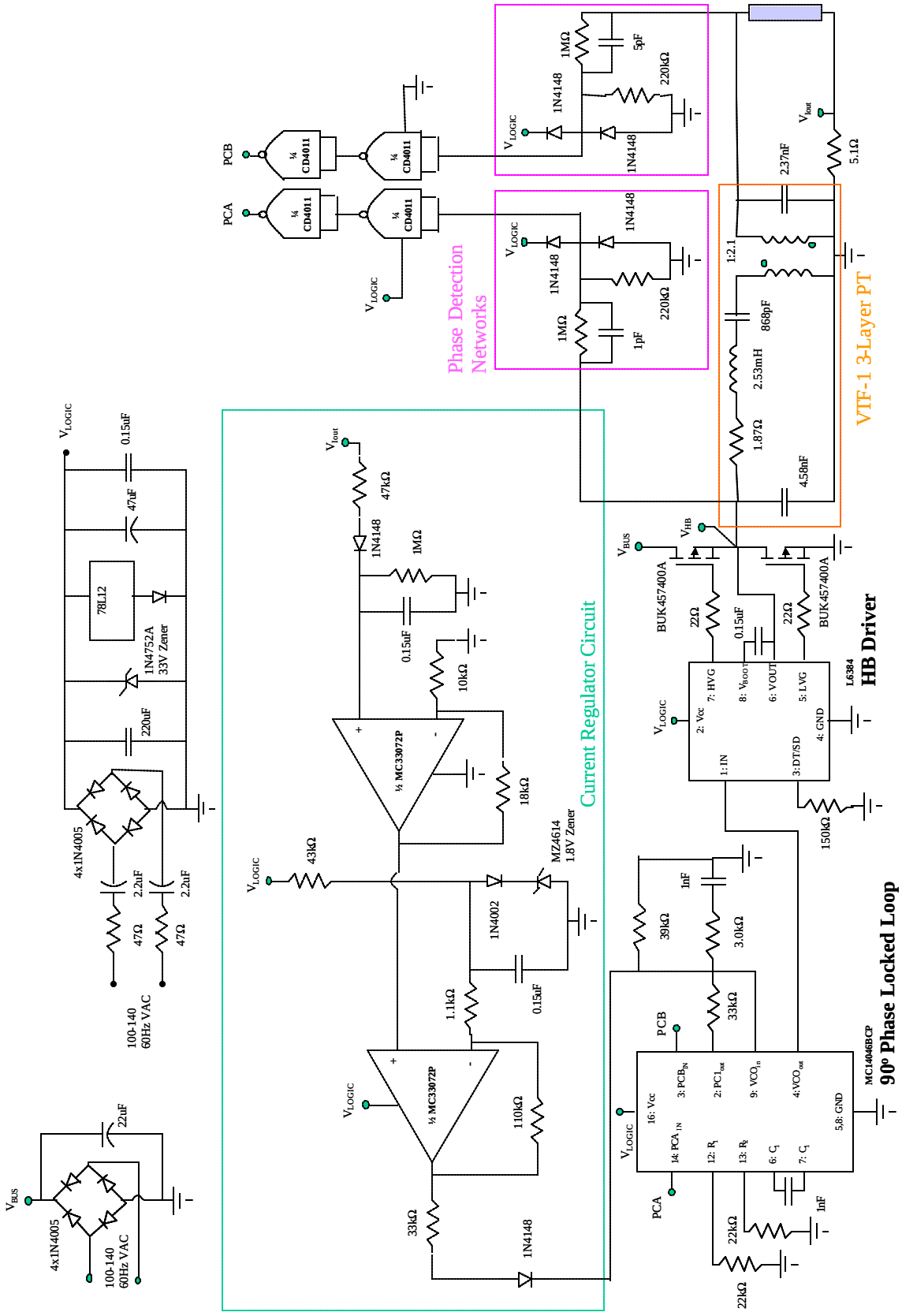

Figure 3.2. Complete non-PFC circuit schematic.

3.4 Circuit Test Results

In an effort to demonstrate the operation of this circuit several waveforms were sampled during circuit operation with a 30-watt lamp power level. The first waveform, Figure 3.3, shows the 60-Hz AC input voltage to the circuit and the respective current. As can be seen from the highly non-linear current, the circuit was in no way designed to operate close to unity power factor. Measurement of the power factor yields an operational point of 0.570 with an input current harmonic distortion equal to 111.9%. Circuit efficiency during sustained operation reached a steady state level of 84.5% after 10-minutes of operation.

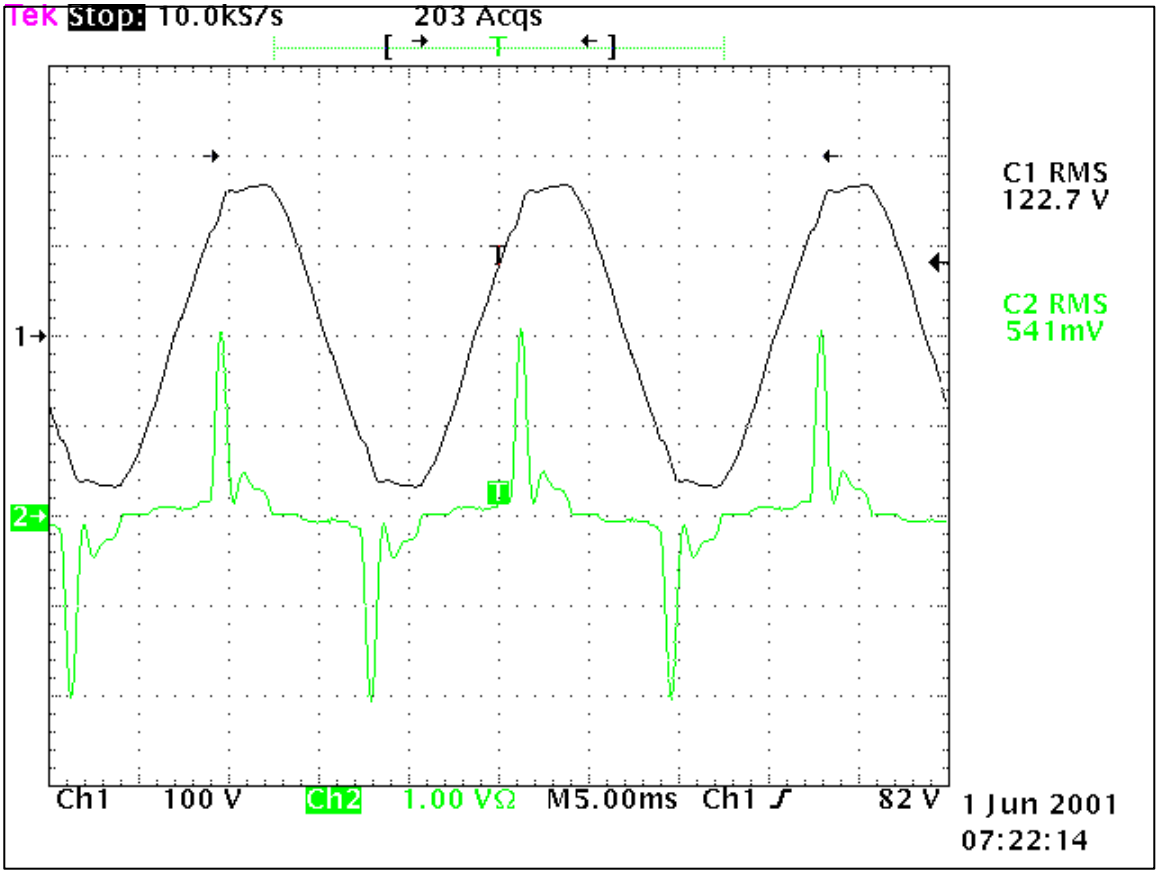

Figure 3.3. Input voltage and current to the non-PFC circuit.

By viewing the voltage that drives the piezoelectric transformer, one can determine whether or not the switches are operating in a zero voltage switching condition. The duty cycle for each switch is set to approximately 25%. During the dead-

time period, the current in the inductor charges/discharges the piezoelectric transformer input capacitor, Cd1 and the MOSFET drain-source capacitances. Here we can see that the voltage transitions in a sinusoidal manor from the bus to ground during one portion of the dead-time period and from ground back to the bus during the other period. At the time when the transition tries to exceed the bus voltage or go below the ground reference, the body diode of the respective MOSFET conducts. During the body diode conduction, the voltage across the switch is virtually zero. If the switch is turned on during this condition the turn-on switching losses are minimized.

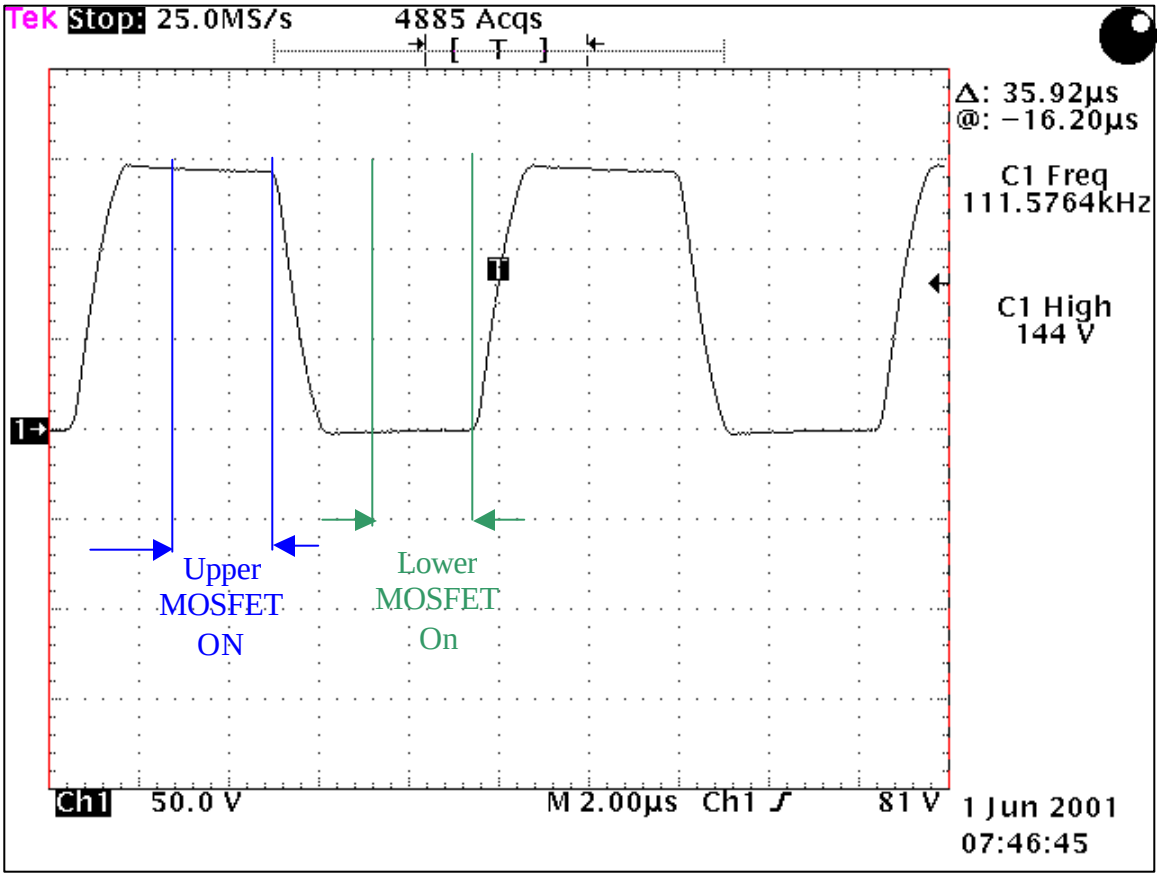

Figure 3.4. Piezoelectric transformer drive voltage displaying ZVS operation.

Lamp voltage and current are shown in Figure 3.5. Here the non-linear nature of the lamp displays itself in the distortion of the current waveform in comparison to the driving voltage waveform. The crest factor of the lamp indicates the ratio of the peak current to the RMS current caused by the 60-Hz line voltage oscillation. Figure 3.6 shows the measured crest factor, which calculated to be approximately 1.45.

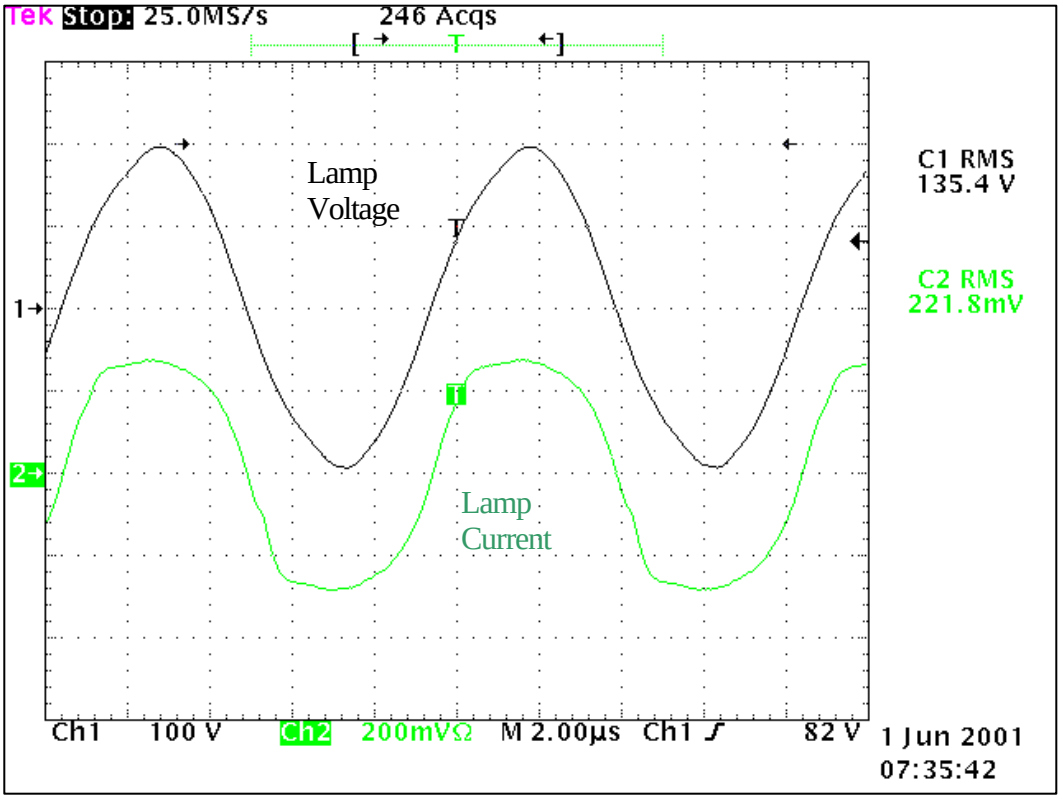

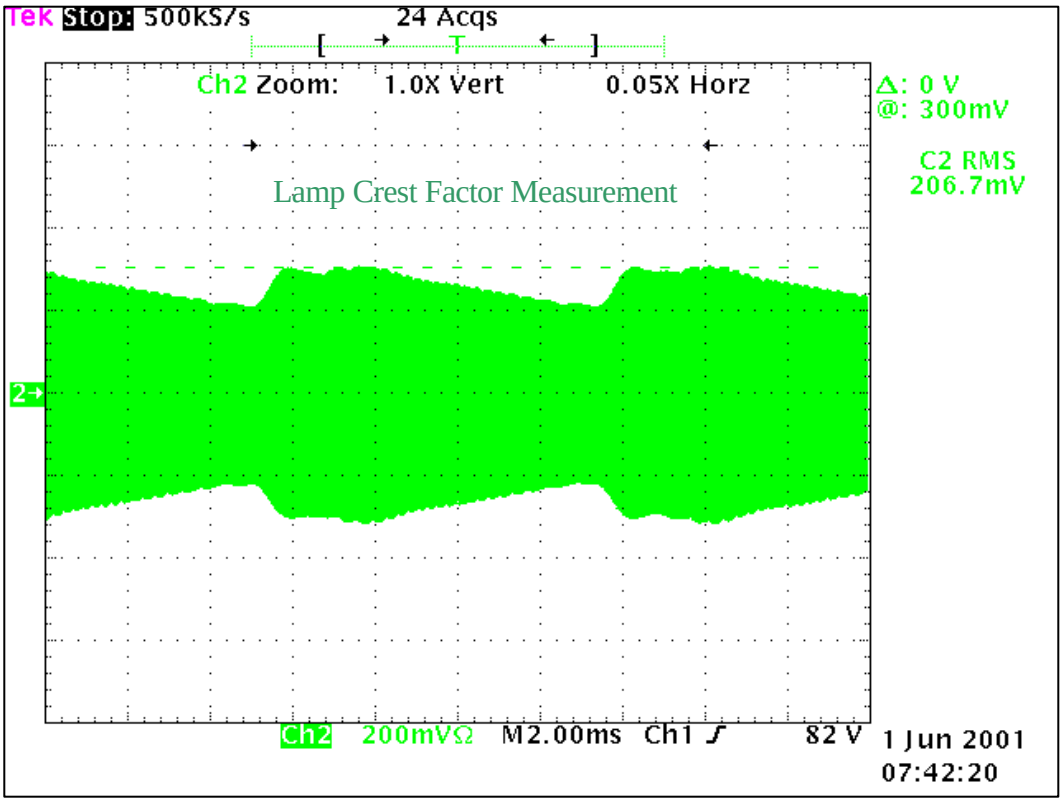

Figure 3.5. Lamp driving voltage and current and lamp crest factor.

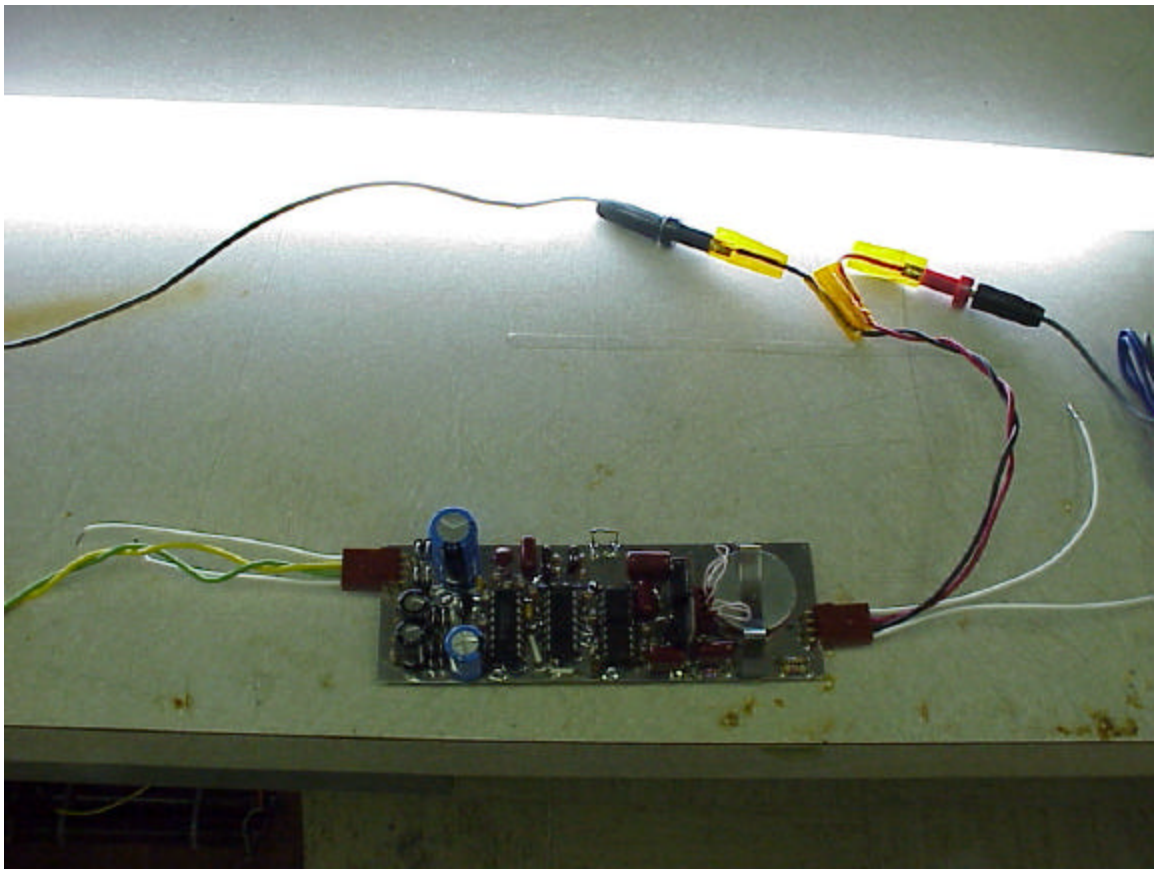

Figure 3.6. Operation of the non-PFC ballast.

Figure 3.6 shows the non-PFC ballast in full-power operation while driving a 32-watt FHF-32 MEW lamp. Notice the mounting of the piezoelectric transformer onto the surface of the circuit board. The technique will be discussed further in the next chapter.

Thermal analysis using a type-T thermocouple adhered directly to the side of the Transoner during testing yielded an initial temperature of 24.0^{o}C with an accompanying efficiency of 86.4%. After 10-minutes the circuit had reached steady state. The final temperature was found to be 72^{o}C with an accompanying efficiency of 84.5%. This represents a 48^{o}C rise in temperature and an approximate 2% decrease in efficiency. Further thermal discussion continues in Chapter 4.

Standard conducted electromagnetic interference, EMI, testing was completed on the circuit yielding common-mode, differential mode, and total measurement results.

Figure 3.7 shows the total EMI for the non-PFC circuit. Figure 3.8 breaks down the total EMI into the separate common mode and differential mode portions. Note that for these measurements there was no EMI filter present, thus these measurements represent the circuit's true EMI characteristic.

In all three plots, the frequency was first swept from 10kHz-150kHz with a bandwidth of only 300Hz. The frequency was then swept from 150kHz-30Mhz with a bandwidth of 30kHz. This method allows very high resolution in the low frequency range. Notice that in all of the plots, the switching frequency, of approximately 110kHz, exists as the strongest component.

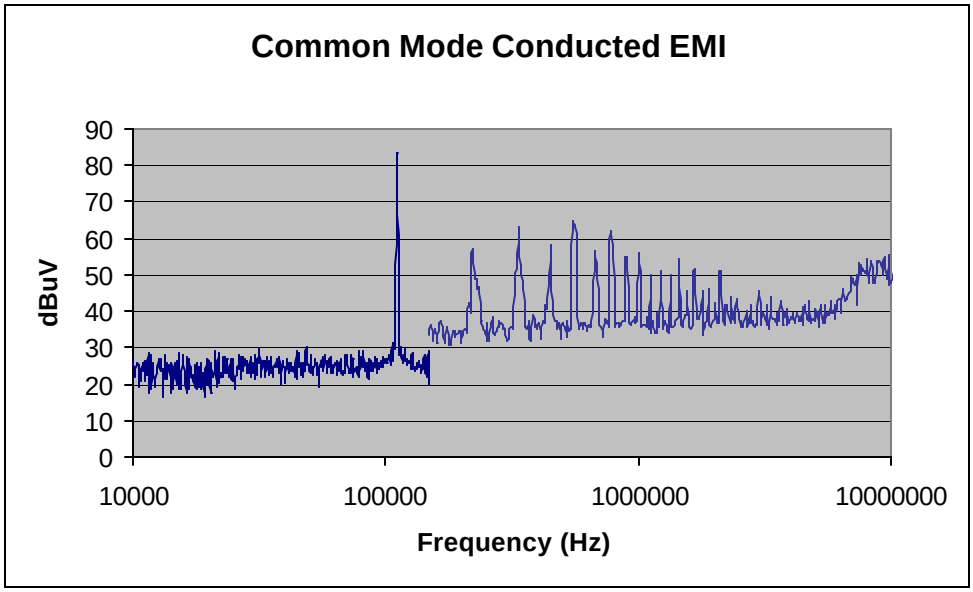

Figure 3.7. Total conducted EMI measurement result during full-power operation.

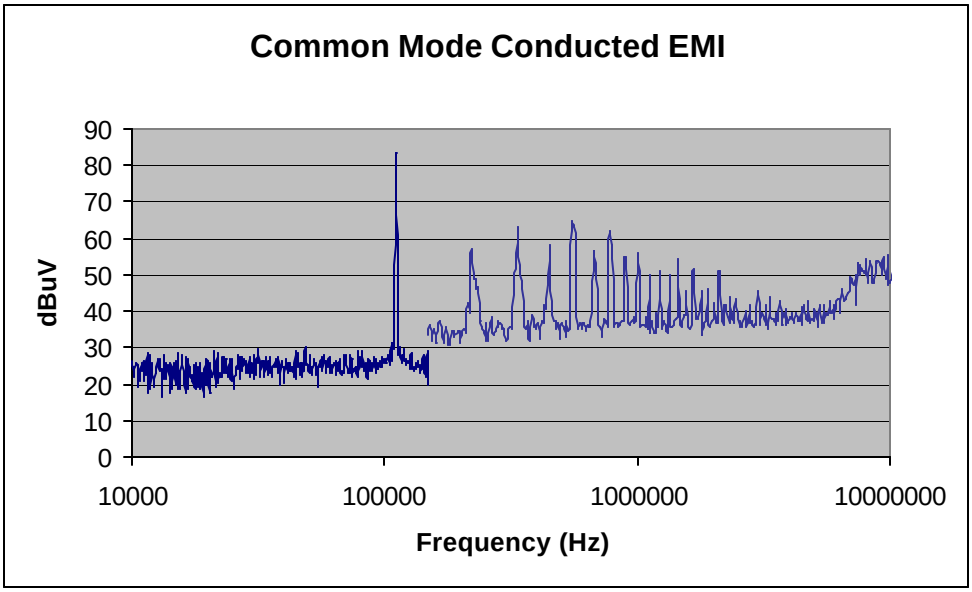

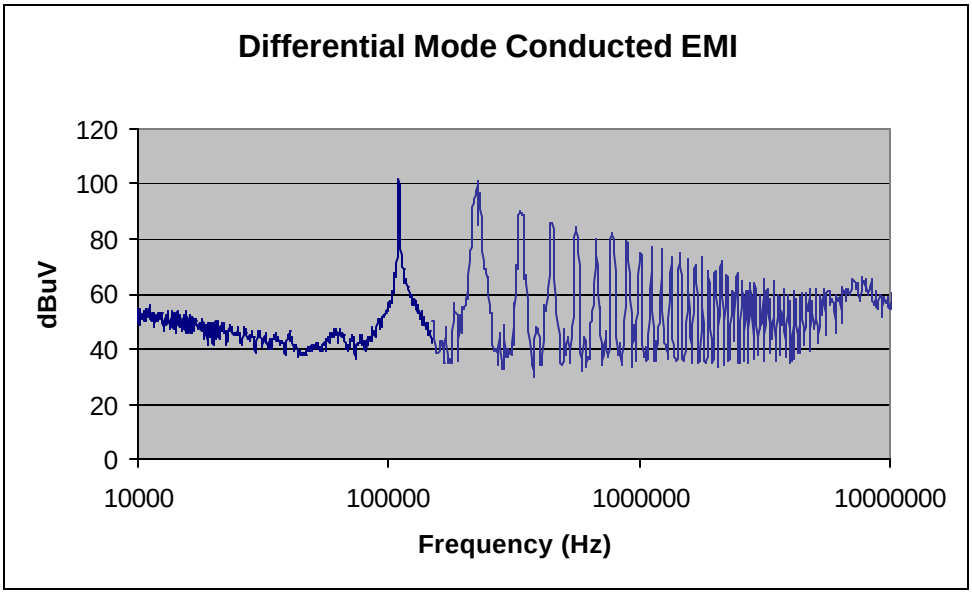

Figure 3.8. Common mode and differential mode conducted EMI measurements result during full-power operation.

3.5 Summary

The design of this circuit has utilized the characteristics of the piezoelectric transformer to enhance the overall performance. The circuit topology operates like a parallel-series resonant converter, thus during lamp ignition a 90^{o} PLL is utilized to lock the input and output phase such that a very high voltage is produced ensuring a quick and

reliable ignition of the lamp. A simple average current controller is utilized to increase the switching frequency as needed to regulate the lamp current.

By carefully designing the piezoelectric transformer as in Chapter 1, the half-bridge switches can be made to operate in a zero-voltage switching condition, which greatly enhances the overall circuit efficiency. During steady state operation, the circuit operates at almost 85% efficiency including the power losses in the linear power supply used in the logic and driver circuitry. The lamp crest factor was shown to be approximately 1.45 which could be further enhanced with the addition of more bulk capacitance at across the main bus power supply rails.

Chapter 4. Thermally Conductive Mounting Technique

4.1 Introduction

The piezoelectric transformer is a device, which converts electrical energy to mechanical energy in the actuator layer(s) and converts mechanical energy back to electrical energy in the transducer layer(s). A diagram of a simple radial mode piezoelectric transformer is shown below as Figure 4.1.

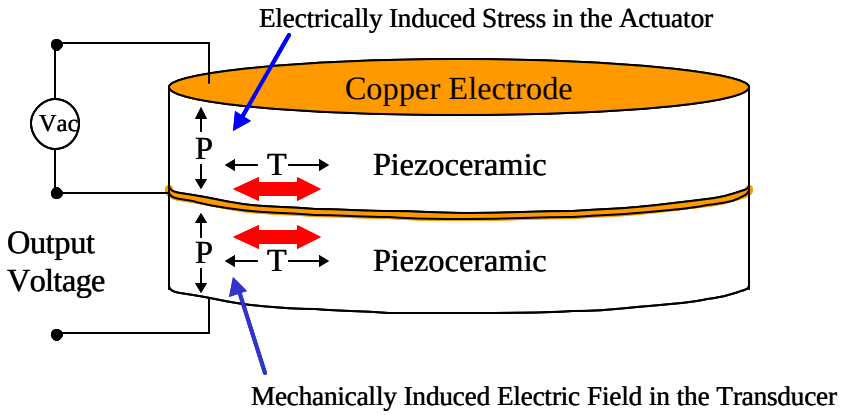

Figure 4.1. Radial mode piezoelectric transformer.

Because the piezoelectric transformer vibrates, any means by which it is adhered to a surface causes loss of energy through the fixing media to the mounting surface as in [12]. The result is a loss in the apparent efficiency due to power that is consumed through the interface. By carefully choosing the interface material to use in the mounting process, two features can be achieved. The first benefit allows virtually no conduction of the mechanical energy to the mounting surface. The second benefit of this new mounting method allows heat conduction from the device to the surface. Figure 4.2 shows a diagram of the physical mounting method.

A spring clip is used to apply force to a metal disk atop the structure. The metal disk evenly distributes the force on the upper interface material. The force is used to provide good thermal contact to both the upper and lower surfaces of the piezoelectric

transformer. The spring connects to the mounting surface thus both providing a mechanical mounting method and a means for thermal conduction.

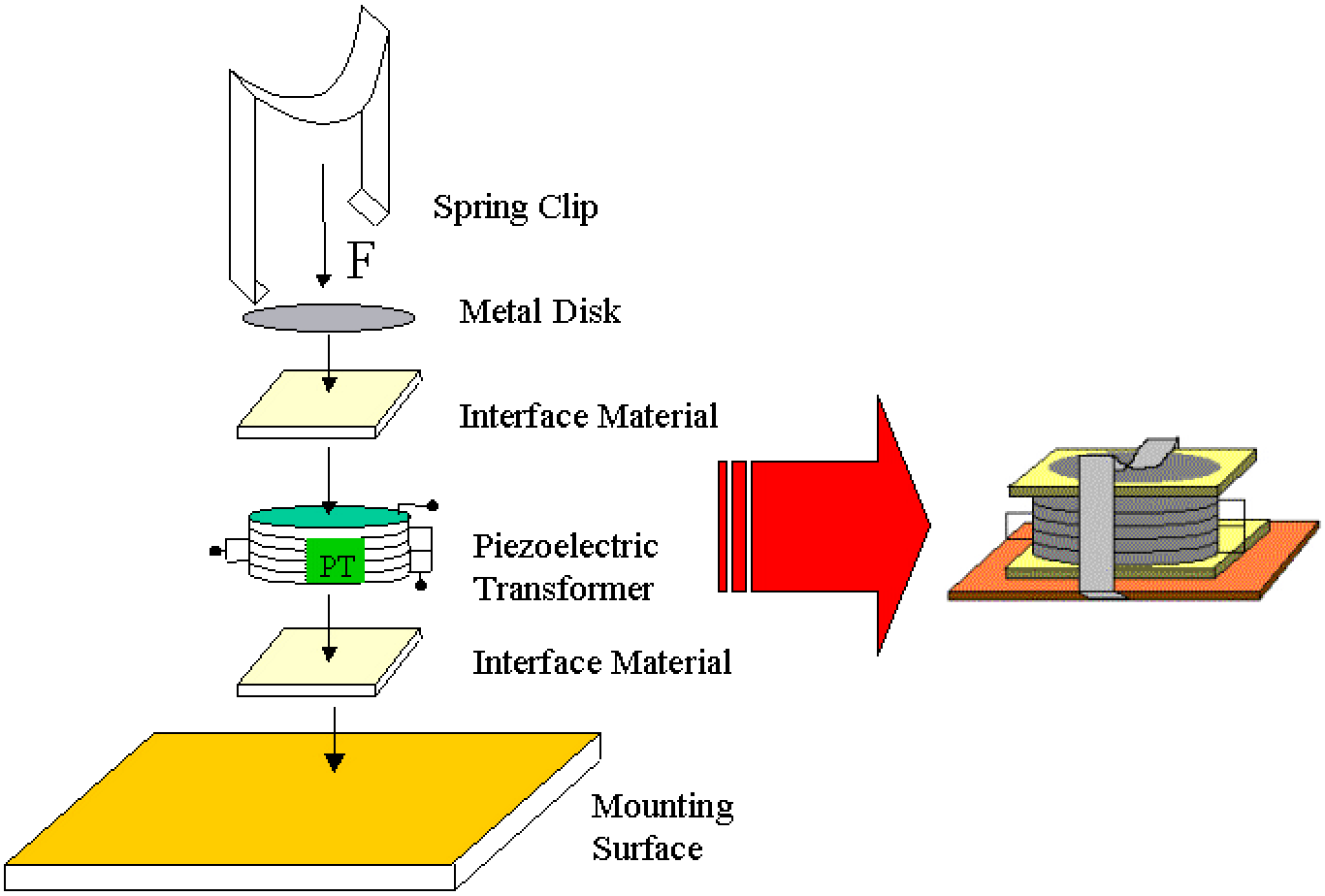

Figure 4.2. Physical construction of interface and piezoelectric transformer

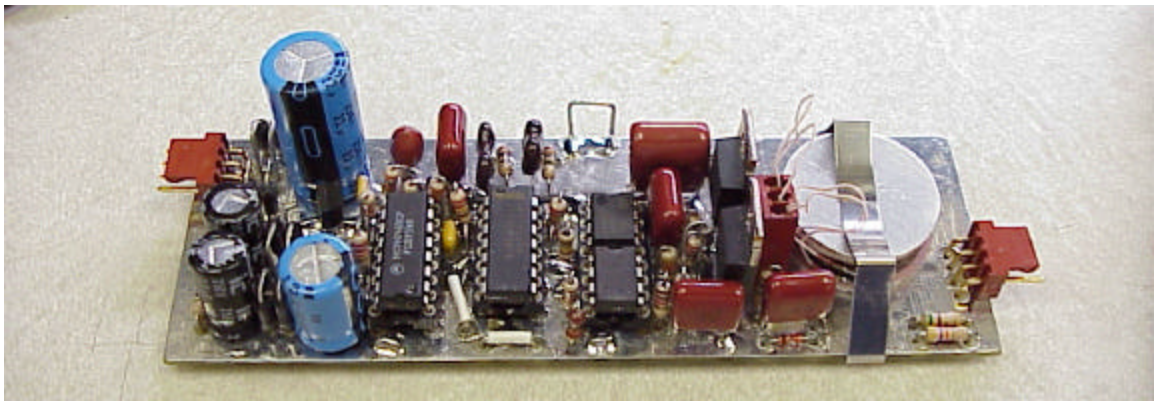

Figure 4.3. Actual mounting of Transoner to PCB.

4.2 Important Considerations

The accepted simplified equivalent circuit model for a piezoelectric transformer is shown as Figure 4.4. The internal resistance, R, represents the potential losses of the piezoelectric transformer via electrical power loss during current conduction. Through experimentation, the internal resistance, R, dramatically increases when the interface material is not chosen correctly. Shown below, as Figure 4.5, is an example of the results of testing several different thermal interface materials with various spring forces applied to the piezoelectric transformer designed in the body of this thesis. The y-axis of the chart shows the change in internal resistance when compared the same piezoelectric transformer in an un-mounted state. The x-axis shows the equivalent applied spring force. Materials, which show the lowest percentage increase in internal resistance, will have the least effect on the electrical performance. The materials used in the testing were samples received from The Bergquist Company [17] and W. L. Gore & Associates, Inc. [18]. Table 4.1 below indicates the exact materials that were tested and the respective abbreviation used in Figure 4.5. Note that some materials have stated thermal resistances that are given at higher pressures. This is due to the non-conforming nature of the materials at low pressure. The thermal resistance at such low pressures can cause extremely high thermal resistances.

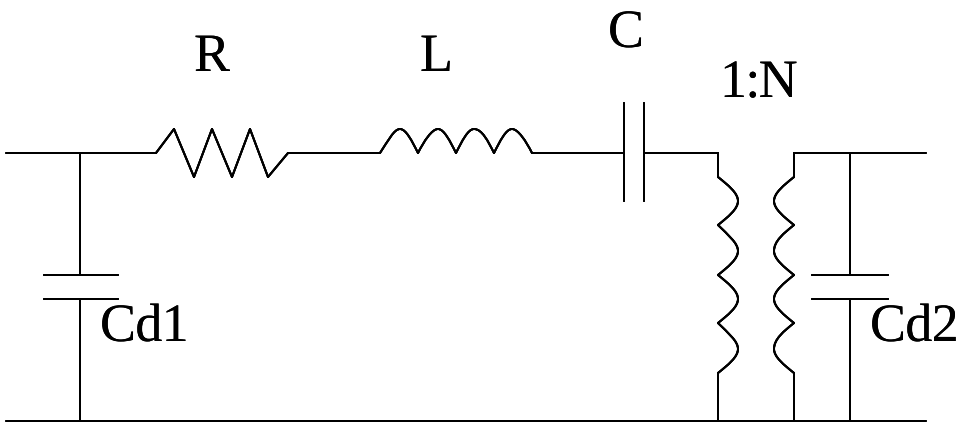

Figure 4.4. Simplified piezoelectric transformer equivalent circuit model.

Table 4.1. Thermal interface materials.

Manufacturer	Material	Thickness	Abbreviation	Rth for 1-in^2
Bergquist	Gap Pad VO Ultra Soft	20mil	VO Ultra 20mil	1.0 °C/W @ 1psi
Bergquist	Gap Pad VO Ultra Soft	60mil	VO Ultra 60mil	3.0 °C/W @ 1psi
Bergquist	Gap Pad VO Ultra Soft	100mil	VO Ultra 100mil	5.0 °C/W @ 1psi
Bergquist	Gap Pad VO Ultra Soft	250mil	VO Ultra 250mil	12 °C/W @ 1psi
Bergquist	Gap Pad 2000	60mil	GP2000 60mil	1.2 °C/W @ 1psi
Bergquist	Gap Pad 2000	125mil	GP2000 125mil	2.5 °C/W @ 1psi
Bergquist	Gap Pad 3000	60mil	GP3000 60mil	0.8 °C/W @ 1psi
Bergquist	Sil Pad 900	15mil	SP900 15mil	0.9 °C/W @ 10psi
Gore	Polarchip CP7003	20mil	CP7003 20mil	1.6 °C/W @ 7psi
Gore	Polarchip CP7003	40mil	CP7003 40mil	3.9 °C/W @ 7psi
Gore	Polarchip CP7003	80mil	CP7003 80mil	7.8 °C/W @ 7psi
Gore	Polarchip CP7003	120mil	CP7003 120mil	11.5 °C/W @ 7psi
Gore	Polarchip CP8000	20mil	CP8000 20mil	2.0 °C/W @ 7psi
Gore	Polarchip CP8000	40mil	CP8000 40mil	3.8 °C/W @ 7psi
Gore	Polarchip CP8000	80mil	CP8000 80mil	8.5 °C/W @ 7psi

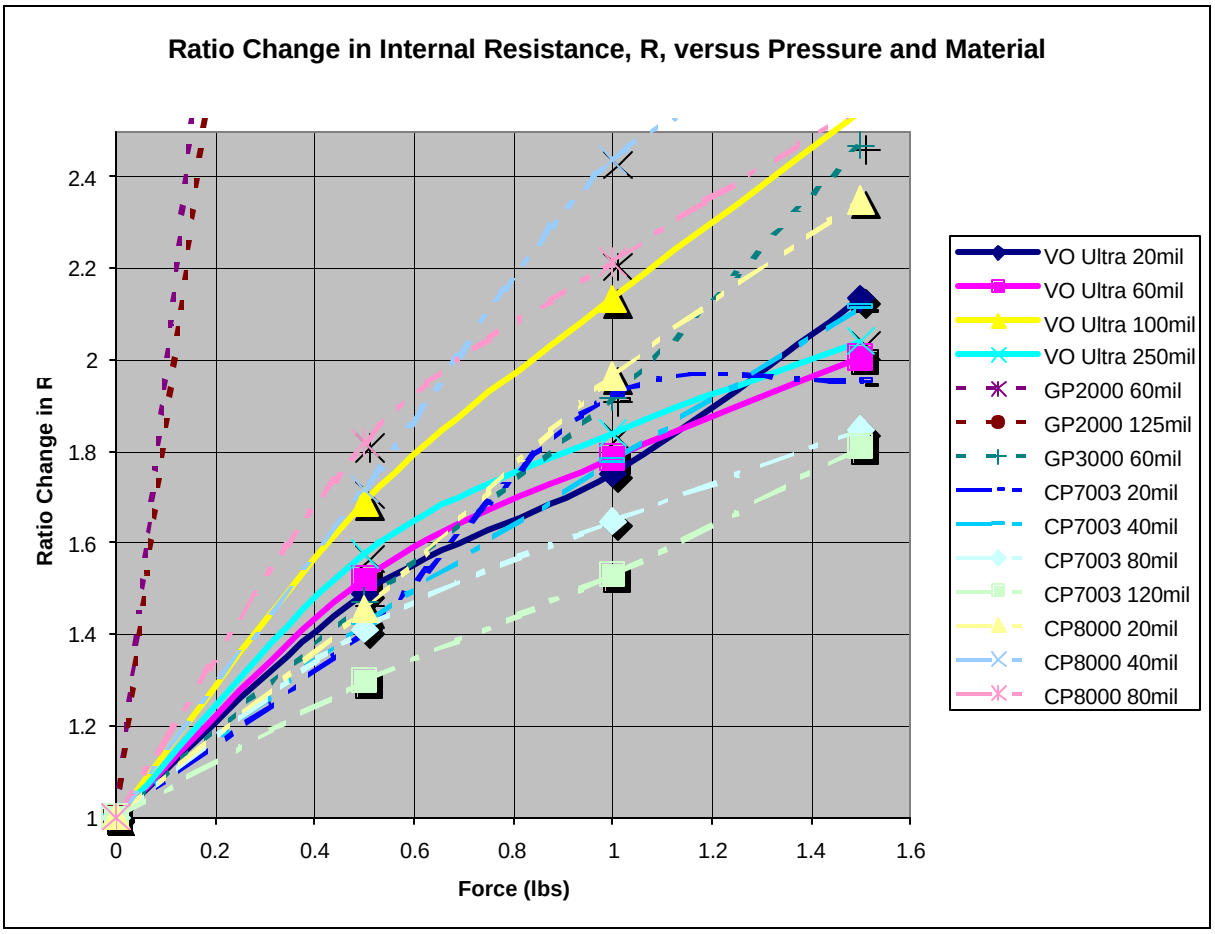

Figure 4.5. Ratio change in internal resistance, R, versus applied force and material.

Notice that the slope of the curves, based on some materials, are much greater than the others. Through experimentation it was discovered that the nature of the interface between the piezoelectric transformer and the thermally conductive material must be such that there is a non-adhesive quality to the interface material. Even a slight "tacky-ness" to the material causes a great increase in losses through the coupling of mechanical energy.

4.3 Test Results

In order to provide a reference for the usefulness of this invention, a 32-watt ballast circuit was constructed with a Face Electronics radial mode piezoelectric transformer. The piezoelectric transformer was mounted as shown in Figure 2 directly to a dual sided copper printed circuit board. At a continuous output of 32-watts the

temperature reached a steady-state level of 48^{o}C above ambient with no forced-air cooling. Testing showed that the steady-state temperature was reached after approximately 10-minutes. In contrast, the same test was performed with the piezoelectric transformer un-mounted on the same printed circuit board. Within 3-minutes the temperature soared to above 100^{o}C at which time the test was aborted to avoid damage to the device.

4.4 Summary

The mounting method described here will change the way that piezoelectric transformers are viewed from industry. It has been thought that not only were the devices difficult to mount, but that the power should be kept very low in order to avoid excessive heating of the device. Before the research described here was completed, the mounting methods for piezoelectric transformers were crude and could not solve the thermal and mechanical issues. Utilizing this simple and cost effective method, reliability of the devices is increased, power output of current devices can be increased, and future designs of piezoelectric transformers can benefit from higher power densities.

Chapter 5. Conclusions and Future Work

Within this thesis, the basic theory behind the radial mode piezoelectric transformer has been introduced. The accepted simplified equivalent circuit model has been shown to exhibit similar characteristics to a parallel-series resonant circuit. The one thing setting the PT apart, from a circuit made up of discrete inductance and capacitance, is the internal resistance and input capacitance. It has been shown that the dielectric losses in the material, does not significantly affect the potential efficiency of the devices throughout the entire resonant frequency range.

The physical-to-electrical design equations have been revealed, as developed by Ray-Lee Lin, for the radial mode piezoelectric transformer. Using these equations, the physical dimensions and material properties can be used to directly calculate the equivalent circuit model parameters. A sample was designed to meet the required voltage gain, ZVS operation, and high efficiency for a 120-volt 60Hz AC input application. This sample was constructed by Face Electronics and tested comparing very well to the theoretical calculations.

A circuit was constructed using the piezoelectric transformer that was designed, in order to prove the viability of the design process. Test results demonstrated the ability of the PT to not only ignite and sustain an FHF-32 lamp, but also provide ZVS for the half-bridge switches, at an efficiency of around 85%.

One solution, for the mounting of a radial mode piezoelectric transformer, has been provided in this thesis. In the past, it has been thought that not only were the devices difficult to mount, but that the power should be kept very low in order to avoid excessive heating of the device. Before the research described here was completed, the mounting methods for piezoelectric transformers were crude and could not solve the thermal and mechanical issues. Utilizing this simple and cost effective method,

reliability of the devices is increased, power output of current devices can be increased, and future designs of piezoelectric transformers can benefit from higher power densities.

Recommended future work in this area should contain an extension of the design process, such that single stage power factor correction may be included. Further work could also entail detailed thermal analysis regarding the mounting technique, which has been described here, and other hypothetical possibilities. Lead attachment to the devices still remains an issue that must be addressed for reliability under the high stress of vibration. With this said, the future of the radial mode piezoelectric transformer looks good, with higher power levels not only possible, but likely, as research in this area continues.

References

[1] Ray-Lee Lin, "Piezoelectric Transformer Characterization and Application of Electronic Ballast," Ph.D Dissertation, Virginia Tech, November 2001.

[2] C. Y. Lin, " Design and Analysis of Piezoelectric Transformer Converters," Ph.D Dissertation, Virginia Tech, July 1997.

[3] T. Zaitsu, "Power Conversion Using Piezoelectric Transformer," Ph.D. Dissertation, Kyushu University, Fukuoka, Japan, August 1997.

[4] Ray L. Lin, Fred C. Lee, Eric M. Baker, and Dan Y. Chen, "Inductor-less Piezoelectric Transformer Ballast for Linear Fluorescent Lamps," Proceedings of CPES Power Electronics Seminar, pp.309-314, Sept. 17-19, 2000.

[5] Eric M Baker, Weixing Huang, Dan Y. Chen, and Fred C. Lee, "Radial Mode Piezoelectric Transformer Design for Fluorescent Lamp Ballast Applications," Proceedings of CPES Power Electronics Seminar, pp.104-112, April 23-25, 2001.

[6] Ray L. Lin, Eric Baker, and Fred C. Lee, "Transoner Characterization", First Quarterly Progress Report, ELC-99-007, August 28, 1999.

[7] Ray L. Lin, Eric Baker, Jia Wei, Dan Y. Chen, and Fred C. Lee, "Transoner Characterization", Second Quarterly Progress Report, ELC-99-007, October 29, 1999.

[8] Ray L. Lin, Eric Baker, Jia Wei, Dan Y. Chen, and Fred C. Lee, "Transoner Characterization", Third Quarterly Progress Report, ELC-99-007, January 31, 2000.

[9] Ray L. Lin, Eric Baker, Jia Wei, Dan Y. Chen, and Fred C. Lee, "Transoner Characterization", Final Report, ELC-99-007, April 30, 2000.

[10] Eric M. Baker, Fengfeng Tao, Weixing Huang, Jinghai Zhou, Dan Y. Chen, and Fred C. Lee, "Linear Ballast Development", First Quarterly Report, ELC-00-006, September 30, 2000.

[11] Eric M. Baker, Jinghai Zhou, Fengfeng Tao, Weixing Huang, Dan Y. Chen, and Fred C. Lee, "Linear Ballast Development", Second Quarterly Report, ELC-00-006, December 30, 2000.

[12] Eric M. Baker, Jinghai Zhou, Weixing Huang, Dan Y. Chen, and Fred C. Lee, "Linear Ballast Development", Third Quarterly Report, ELC-00-006, February 28, 2001.

[13] Eric M. Baker, Jinghai Zhou, Weixing Huang, Dan Y. Chen, and Fred C. Lee, "Linear Ballast Development", Final Report, ELC-00-006, May 31, 2001.

[14] MC14046B Data Sheet, Motorola Inc., 1997.

[15] L6384 Data Sheet, ST Microelectronics, Dec. 1999.

[16] APC International Ltd., "APC 841-Lead Zirconate Titanate, http://www.americanpiezo.com

[17] http://www.bergquistcompany.com

[18] http://www.gore.com

Appendix A. MathCAD Program to Generate Two-Dimensional Projections for the VTB-1 Radial Mode Piezoelectric Transformer

This program will calculate the performance of a PT and its ability to work in ZVS by matching a choosed load impedance and resonance frequency to a single secondary layer and then varying the primary layer thickness and number.

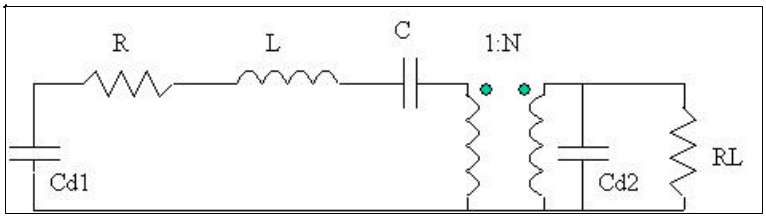

Given the load impedance (RL), output voltage, and supply voltage find the necessary physical dimensions for the radial mode piezoelectric transformer.

Piezoceramic Material Characteristics: APC841

$\rho := 7.6\cdot 10^{-3}\cdot\frac{kg}{cm^3}$ Material Density

$\varepsilon_0 := 8.85418781761\cdot 10^{-12}\cdot\frac{farad}{m}$ Permittivity of Free Space

$\varepsilon_{33} := 1350\cdot\varepsilon_0$ Permittivity of the Material

$Qm := 1400$ Mechanical Quality Factor

$k_{31} := 0.33$

$k_{33} := 0.68$ Coupling Coefficients

$d_{31} := -109\cdot 10^{-12}\cdot\frac{m}{volt}$

$d_{33} := 275\cdot 10^{-12}\cdot\frac{m}{volt}$ Piezoelectric Coefficients

$S_{11} := 11.7\cdot 10^{-12}\cdot\frac{m^2}{newton}$

$S_{33} := 17.3\cdot 10^{-12}\cdot\frac{m^2}{newton}$ Elastic Compliance

$N_l := 1700\cdot\frac{m}{s}$ Longitudinal Frequency Constant

$N_t := 2005\cdot\frac{m}{s}$ Thickness Frequency Constant

$N_p := 2055\cdot\frac{m}{s}$ Radial Frequency Constant

$\tan\delta := 0.005$ $C_f := 1$

$\tan\delta := \tan\delta\, C_f$

Correction Factor for the material dissipation loss due to the specification being given at 1kHz

Note: When calculating the resonance frequency of th PT, the manufacture's rated material wavespeed may need to be modified in order for agreement to exist between:

Input the steady-state load impedance, power level, and source voltage:

$RL := 500\cdot ohm$ Steady state load impedance of the FHF32 Lamp at 32W

$Vbus := 155\cdot volt$

$Plamp := 32\cdot watt$

Begin the Calculations:

$Vlamp := \sqrt{PlampRL}$ $\quad Vlamp = 126.491\,V$ RMS sinusoidal lamp voltage

Assuming that the input voltage to the PT is a trpezoidal waveform, we can approximate the amplitude of the fundamental driving frequency as follows:

$Vpt := 0.4\,Vbus$ RMS sinusoidal PT input voltage

Thus the desired gain will be as follows:

$Av_{min} := \frac{Vlamp}{Vpt}$ $\quad Av_{min} = 2.04$

$N_1 := 2$ $\quad N_2 := 1$ $\quad N := \frac{N_1}{N_2}$

For maximum efficiency: $\frac{1}{\omega_s \cdot Cd2} = RL$

Set the working frequency range:

$f_{min} := 90000\,Hz$

$f_{max} := 130000\,Hz$

$npts := 50$

$n := 1..npts$

$f_n := f_{min} + \frac{(f_{max} - f_{min})}{npts - 1} \cdot (n - 1)$ $\quad N_p = 2.055 \times 10^3\,\frac{m}{s}$

Given that the radius of the material is directly related to the radial mode fundamental frequency, choose the approximate resonance frequency yielding the radius:

$f_r := 100000\,Hz$ $\quad r := 0.5\frac{N_p}{f_r}$ $\quad r = 0.405\,in$

$\frac{0.825}{2} = 0.413$ $\quad r := \frac{0.825\,in}{2}$

Material with a diameter of 825mil is commonly available and will be used in this design process.

$Cd2 := \frac{1}{2 \cdot \pi \cdot 1 \cdot 10^5 \cdot Hz\,RL}$ $\quad Cd2 = 3.183 \times 10^{-9}\,F$

Now we can solve for the secondary thickness:

$$Cd2 = \frac{N_2 \cdot \pi \cdot r^2 \cdot \varepsilon_{33} \cdot \left(1 - \frac{d_{31}^2}{\varepsilon_{33} \cdot S_{11}}\right)}{t_2} \qquad t_2 := \frac{N_2 \cdot \pi \cdot r^2 \cdot \varepsilon_{33} \cdot \left(1 - \frac{d_{31}^2}{\varepsilon_{33} \cdot S_{11}}\right)}{Cd2} \qquad t_2 = 0.047\,in$$

Now choose a range for the primary thickness: $r = 0.413in$ $t_2 := 0.050 \cdot in$ Available Material

$t_{1min} := 0.01 \cdot in$

$t_{1max} := 0.2 \cdot in$

$npts2 := 100$

$m := 1 .. npts2$

$$t1_m := t_{1min} + \frac{(t_{1max} - t_{1min})}{npts2 - 1} \cdot (m - 1) \qquad C_{Ext} := 1 \cdot 10^{-12} \cdot farad$$

$$Cd2 := \frac{N_2 \cdot \pi \cdot r^2 \cdot \varepsilon_{33} \cdot \left(1 - \frac{d_{31}^2}{\varepsilon_{33} \cdot S_{11}}\right)}{t_2} \qquad Cd2 = 2.97 \times 10^{-9} F$$

The rows are the resultant in varying the frequency, while the columns are the resultant of varying the thickness.

$$Cd1_m := \frac{N_1 \cdot \pi \cdot r^2 \cdot \varepsilon_{33} \cdot \left(1 - \frac{d_{31}^2}{\varepsilon_{33} \cdot S_{11}}\right)}{t1_m} + C_{Ext} \qquad C_m := \frac{8 \cdot (2 \cdot r) \cdot r \cdot (d_{31} \cdot N)^2}{\pi \cdot S_{11} \cdot (N_1 \cdot t1_m + N_2 \cdot t_2)} \qquad R_{Cd1_{n,m}} := \frac{1}{2 \cdot \pi \cdot f_n \cdot Cd1_m \cdot \tan\delta}$$

$$R_m := \frac{\sqrt{2 \cdot \rho \cdot S_{11}^3} \cdot (N_1 \cdot t1_m + N_2 \cdot t_2)}{16 \cdot r \cdot Qm \cdot (N \cdot d_{31})^2} \qquad L_m := \frac{(2 \cdot r) \cdot \rho \cdot S_{11}^2 \cdot (N_1 \cdot t1_m + N_2 \cdot t_2)}{16 \cdot \pi \cdot r \cdot (N \cdot d_{31})^2} \qquad R_{Cd2_n} := \frac{1}{2 \cdot \pi \cdot f_n \cdot Cd2 \cdot \tan\delta}$$

The input and output capacitances exhibit dielectric losses which are represented by the parallel resistances

$$Av_{n,m} := \left| \left[\frac{1}{N} \cdot \frac{\frac{RL \cdot \left[\left(R_{Cd2_n}\right)^{-1} + 2 \cdot \pi \cdot i \cdot f_n \cdot Cd2 \right]^{-1}}{RL + \left[\left(R_{Cd2_n}\right)^{-1} + 2 \cdot \pi \cdot i \cdot f_n \cdot Cd2 \right]^{-1}}}{R_m + 2 \cdot \pi \cdot i \cdot f_n \cdot L_m + \frac{1}{2 \cdot \pi \cdot i \cdot f_n \cdot C_m} + \frac{1}{N^2} \cdot \frac{RL \cdot \left[\left(R_{Cd2_n}\right)^{-1} + 2 \cdot \pi \cdot i \cdot f_n \cdot Cd2 \right]^{-1}}{RL + \left[\left(R_{Cd2_n}\right)^{-1} + 2 \cdot \pi \cdot i \cdot f_n \cdot Cd2 \right]^{-1}}} \right] \right|$$

$Cd1_{27} = 4.96 \times 10^{-9} F$

$R_{27} = 1.908\Omega$

$L_{27} = 3.757 \times 10^{-3} H$

$C_{27} = 5.266 \times 10^{-10} F$

$Cd2 = 2.97 \times 10^{-9} F$

$N = 2$

$$Zin_{n,m} := \left[\frac{\left[\left(R_{Cd1_{n,m}}\right)^{-1} + 2\cdot\pi\cdot i\cdot f_n\cdot Cd1_m\right]^{-1}\cdot\left[R_m + \frac{1}{2\cdot\pi\cdot i\cdot f_n\cdot C_m} + 2\cdot\pi\cdot i\cdot f_n\cdot L_m + \frac{1}{N^2}\cdot\frac{RL\cdot\left[\left(R_{Cd2_n}\right)^{-1} + 2\cdot\pi\cdot i\cdot f_n\cdot Cd2\right]^{-1}}{RL + \left[\left(R_{Cd2_n}\right)^{-1} + 2\cdot\pi\cdot i\cdot f_n\cdot Cd2\right]^{-1}}\right]}{\left[\left(R_{Cd1_{n,m}}\right)^{-1} + 2\cdot\pi\cdot i\cdot f_n\cdot Cd1_m\right]^{-1} + \left[R_m + \frac{1}{2\cdot\pi\cdot i\cdot f_n\cdot C_m} + 2\cdot\pi\cdot i\cdot f_n\cdot L_m + \frac{1}{N^2}\cdot\frac{RL\cdot\left[\left(R_{Cd2_n}\right)^{-1} + 2\cdot\pi\cdot i\cdot f_n\cdot Cd2\right]^{-1}}{RL + \left[\left(R_{Cd2_n}\right)^{-1} + 2\cdot\pi\cdot i\cdot f_n\cdot Cd2\right]^{-1}}\right]} \right]$$

An inductive impedance is a necessary condition for ZVS. However, our system must also satisfy a sufficient condition:

At the time the switches each turn off, there must be enough current in the inductor to charge/discharge both Cd1 and C.

$$ZLCR_{n,m} := \left[\left(R_m\right) + \frac{1}{2\cdot\pi\cdot i\cdot f_n\cdot C_m} + 2\cdot\pi\cdot i\cdot f_n\cdot L_m + \frac{1}{N^2}\cdot\frac{RL\cdot\left[\left(R_{Cd2_n}\right)^{-1} + 2\cdot\pi\cdot i\cdot f_n\cdot Cd2\right]^{-1}}{RL + \left[\left(R_{Cd2_n}\right)^{-1} + 2\cdot\pi\cdot i\cdot f_n\cdot Cd2\right]^{-1}} \right]$$

This is the impedance of the PT without the input capacitance, CD1.

$$\frac{1}{2}\cdot L\cdot \Delta i_L^{\,2} \geq \frac{1}{2}\cdot Cd1\cdot Vbus^2\cdot\left(1 + \frac{Cd1}{C}\right)$$

$$\Delta i_{Lcritical_{n,m}} := \sqrt{\frac{Cd1_m\cdot\left(C_m + Cd1_m\right)}{L_m\cdot C_m}}\cdot Vbus$$

Now let's calculate the instantaneous value ofΔ iL during the switch turn-off time:

$$\Delta i_{L_{n,m}} := \frac{Vbus\cdot\frac{2}{\pi}}{\left|ZLCR_{n,m}\right|}\cdot\frac{\sin(\pi\cdot 0.25)}{\pi\cdot 0.25}\cdot\sin\left(\arg\left(ZLCR_{n,m}\right)\right)$$

Let's also consider the efficiency:

$$Eff_{min} := 0.95$$

$$Pin_{n,m} := Re\left(\frac{1}{Zin_{n,m}}\right)$$

$$Pout_{n,m} := \frac{\left(Av_{n,m}\right)^2}{RL}$$

$$Eff_{n,m} := \frac{Pout_{n,m}}{Pin_{n,m}}$$

$Eff_{min} = 0.95$

$$Av_{n,m} := \begin{cases} 1 & \text{if } Av_{n,m} \geq Av_{min} \\ 0 & \text{otherwise} \end{cases} \qquad Eff_{n,m} := \begin{cases} 1 & \text{if } Eff_{n,m} \geq 0.90 \\ 0 & \text{otherwise} \end{cases} \qquad \Delta iL_{n,m} := \begin{cases} 1 \cdot A & \text{if } \Delta iL_{n,m} \geq \Delta iLcritical_{n,m} \\ 0 & \text{otherwise} \end{cases}$$

$$Sol_{n,m} := \begin{cases} 1 & \text{if } \left(Av_{n,m} + Eff_{n,m} + \Delta iL_{n,m} \cdot \frac{1}{A} \right) = 3 \\ 0 & \text{otherwise} \end{cases}$$

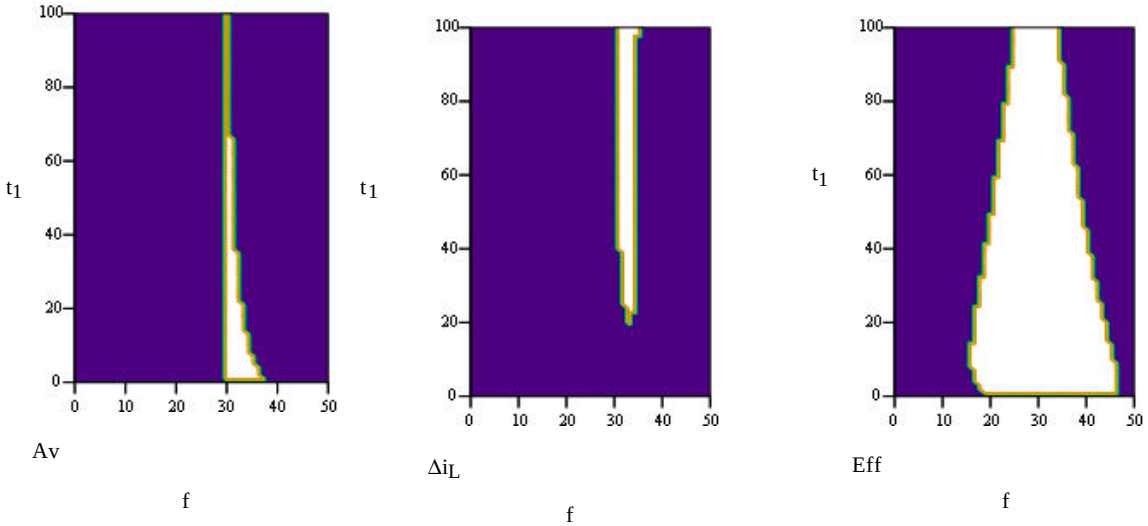

$t1_{100} = 0.2\,in$

$t1_{80} = 0.162\,in$

$t1_{60} = 0.123\,in$

$t1_{40} = 0.085\,in$

$t1_{20} = 0.046\,in$

$t1_{0} = 0\,in$

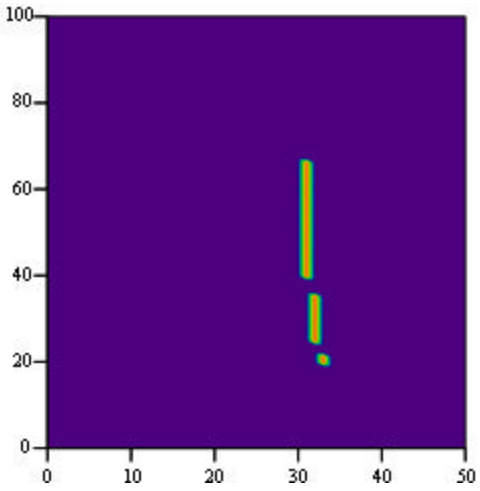

Sol

$f_0 = 0\,Hz$

$f_{10} = 9.735 \times 10^4\,Hz$

$f_{20} = 1.055 \times 10^5\,Hz$

$f_{30} = 1.137 \times 10^5\,Hz$

$f_{40} = 1.218 \times 10^5\,Hz$

$f_{50} = 1.3 \times 10^5\,Hz$

Possible Solution #1:	Possible Solution #2:
Material APC 841	Material APC 841
>90% eff	>90% eff
1nF Cext	5nF Cext
fr = 112kHz	fr = 108kHz
N1=2	N1=3
N2=1	N2=1
t1=0.08in	t1=0.06in
t2=0.05in	t2=0.05in
d=0.825in	d=0.825in
total t = 0.21in	total t = 0.23in

Vita

Eric Matthew Baker

The author was born in Richmond, Virginia, in 1971. He received his first bachelor's degree in physics with a minor in mathematics, from Longwood College, in May of 1994. He went on to study at Virginia Polytechnic and State University where he obtained his second bachelor's degree in electrical engineering, concentrating in electronics and networks, in May of 1999.

Three years later, the author received his master's degree in electrical engineering, concentrating in the study of power electronics. His research centered on the design of radial mode piezoelectric transformers and the associated circuitry for fluorescent lamp ballast applications.